Ionics
https://doi.org/10.1007/s11581-019-02874-0

REVIEW

Review of carbon-based electrode materials for supercapacitor energy storage

Richa Dubey[1] · Velmathi Guruviah[1]

Received: 26 April 2018 / Revised: 13 August 2018 / Accepted: 27 August 2018

Abstract

In today's nanoscale regime, energy storage is becoming the primary focus for majority of the world's and scientific community power. Supercapacitor exhibiting high power density has emerged out as the most promising potential for facilitating the major developments in energy storage. In recent years, the advent of different organic and inorganic nanostructured materials like nano carbons, metal oxides, nanosheets of graphene, and conducting polymers has enabled high-performance-fabricated devices. A review of different carbon-based materials used in the fabrication of electrodes for electrochemical capacitors is presented in this paper. Along with materials used, a brief overview of different types of supercapacitors depending on charge storage mechanism is also been discussed. Materials summary including applications have been provided through the exhaustive analysis of the literature. Keeping nano-architecture electrodes in view, a summary of different technologies considering the integration of metal oxide into carbon nanofibers, carbon fiber papers, graphene/reduced graphene oxide, and SWCNTs/MWCNTS has been presented in this work. The specific capacitance in the range of 40–300 F/g had been reported in the literature for the EDLC (electric double-layer capacitors) supercapacitors. In contrast to this, carbon nanomaterials-based metal-oxides supercapacitors (CNMO-SC) have emerged as the new promising candidate which possess large specific capacitance (> 100 F/g), high energy density, and cost effectiveness. Hence, a review of certain types of carbon nanomaterials has also been reported here.

Keywords Carbon nanomaterial-based-metal-oxide supercapacitor · Carbon nanotubes · EDLC (electric double-layer capacitor) · Nanocomposites · Supercapacitor

Introduction

The acceleration at an alarming rate in the global energy consumption along with the carbon dioxide (CO_2) emission has resulted from the increase in the world population, global economic expansion, and greater reliance of human being on energy-consuming appliances [1, 2]. As per the estimation of the World Energy Council, by 2050, the world will require to double its energy supply (www.worldenergy.org). This poses several serious challenges to the human health, environment energy, and security and thereby revealing a need to develop some high-power and power sustainable energy conversion and storage systems like batteries and supercapacitors for different applications ranging from the consumer opto-electronics to hybrid vehicles (electric) with very low exhaust emissions [2, 3].

Energy storing devices act as a major key to handle the problems occurring in renewable energy resources and thereby increasing transmitted power from wind, tidal, etc., into the power grid system. Supercapacitors also known as the ultracapacitors are the electrochemical devices combining the power delivery capability and charge storage capability of conventional capacitors available and the batteries respectively [1–3]. New frontiers are being opened by the recent technology which offered new materials and technologies for the energy storage devices. In particular, the carbon-based nanomaterials like graphene, carbon nanosheets, nonporous carbon, carbon nanotubes, activated carbon, carbon aerogels, metal oxides, conducting polymers, and polymer composites have played significant role in the highly efficient supercapacitors [4, 5].

✉ Velmathi Guruviah
velmathi.g@vit.ac.in

Richa Dubey
richa.dubey2016@vitstudent.ac.in

[1] SENSE Department, VIT University, Chennai, TN 600127, India

Published online: 18 February 2019

Conducting polymers' (CPs) discovery has shown them as a promising candidate for various applications like sensors, LEDs, batteries, photovoltaics, and supercapacitors. CPs used in nanostructured form improved the device performance. A high specific surface area was offered by the nanoscale CPs which helped in improving the redox-meditated charge storage capacity in the energy storage devices. Huge numbers of routes are suggested for synthesizing CP nanostructures. Few of them include electro spinning, self-assembly, template synthesis, interfacial polymerization, and chemical reactions. Among all, template synthesis serves as the most effective synthesis route for many polymers [6]. The appropriate selection of template helps in controlling the length, diameter, and homogeneity of the polymer fiber tubes, thereby making it a simple and cheap process. Due to its high specific surface area and very effective charge storage transport properties, the vertical TNTs (titanium oxide nanotubes) have gained much attention. Semiconducting TNTs as templates offer good conductivity to polymers that were formed in them. This striking advantage made it a prospective template for the growth and development of nanostructured CPs.

The semiconducting nature of TNTs helped in precursor's nucleation which was infiltrated into the tube walls. However, this had an associated disadvantage of complicating the electrochemical filling of tubes. Hence, the interdigitated polymeric 1D 1NS (nano structure) formation remains a big challenge. Studies in the literature survey suggested that the success in template-assisted growth of 1D polymer nanostructure has influence on the effective interactions between the infiltrating polymer and tubular walls of TNT. Another suggested fundamental factor for the formation of 1D nanostructure is the inculcation of monomer concentration [6]. Studies suggested the formation of rigid nanostructure in high monomer concentration and long and nanoporous switch nanostructure with low monomer concentration. Figure 1 represents the growth mechanism of the 1D PTh-NFs (polythiopene-nanofibers) from 1D TNTs with the help of controlled electro polymerization synthesis route [6].

A core challenge in the designing of supercapacitor is the scalable fabrication of electrode while maintaining the high electrochemical performance. PANI (polyanniline)-conjugated polymer possessing redox ability, thermal stability, high conductivity, and good environmental stability is one of the most promising candidates for pseudocapacitive electrode material. Graphene can act as a current collector and can also accommodate enormous amount of charge arising from electrostatic interactions, thereby enhancing the overall electrochemical performance of the hybrid composites. A wide variety of synthesis routes have been suggested for graphene/PANI composites such as electro-polymerization and in situ polymerization. But the mixing of binder or additives for producing electrodes significantly affected the electrical conductivity and structural organization. Hence, there is an increasing

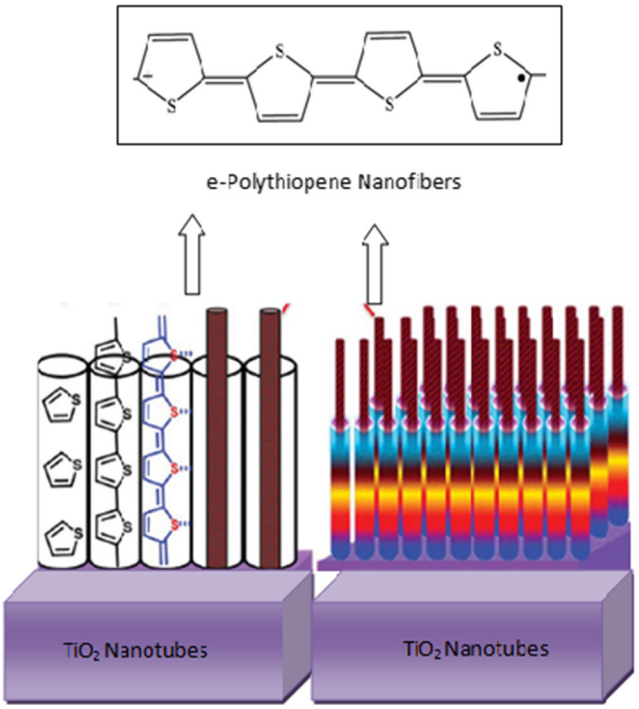

Fig. 1 Schematic representation of the 1D PTh-NFs grown from 1D TNTs by controlled electro polymerization [6]

demand for supercapacitors consisting of binder-free electrodes with good cyclic stability for applications in foldable electronic items. Free-standing electrodes were reported to be prepared in the past using non-covalent deposition of PANI on the film of graphene that were readily worn off irrespective of electrochemical cycling and repeated ionic interactions.

The mixing of graphene oxide and PANI helped in fast and scalable production of graphene/PANI film, but it had an associated drawback. There was a loss in stability and structural consistency, and apart from these, the post-reduction processes for graphene oxide in the resulting polymer composite were complex. Few authors [7] have developed a sequential series of strategies for the fabrication of 3D composites using the hierarchical self assembly which is shown in Fig. 2. In this, there was an attachment of positively charged PANI nanospheres with negatively charged GO sheets via hierarchical self assembly process.

For maximization of the capacitive power, the in-situ reduction route was used which utilized the exposed surfaces of both materials [7]. The observed capacitance for binder-free stand alone graphene/PANI composite was 448 F g^{-1} (at 1 Ag^{-1}) which was quite large in compared to other graphene/conducting polymer films prepared by using any other methods (physical or chemical). The different physical-chemical, structural, and morphological characterizations were used for the determination of the electrochemical performance of the 3D graphene/PANI composites.

The modification of side walls of CNT by using chemical functionalization and/or attachment of suitable nanostructures

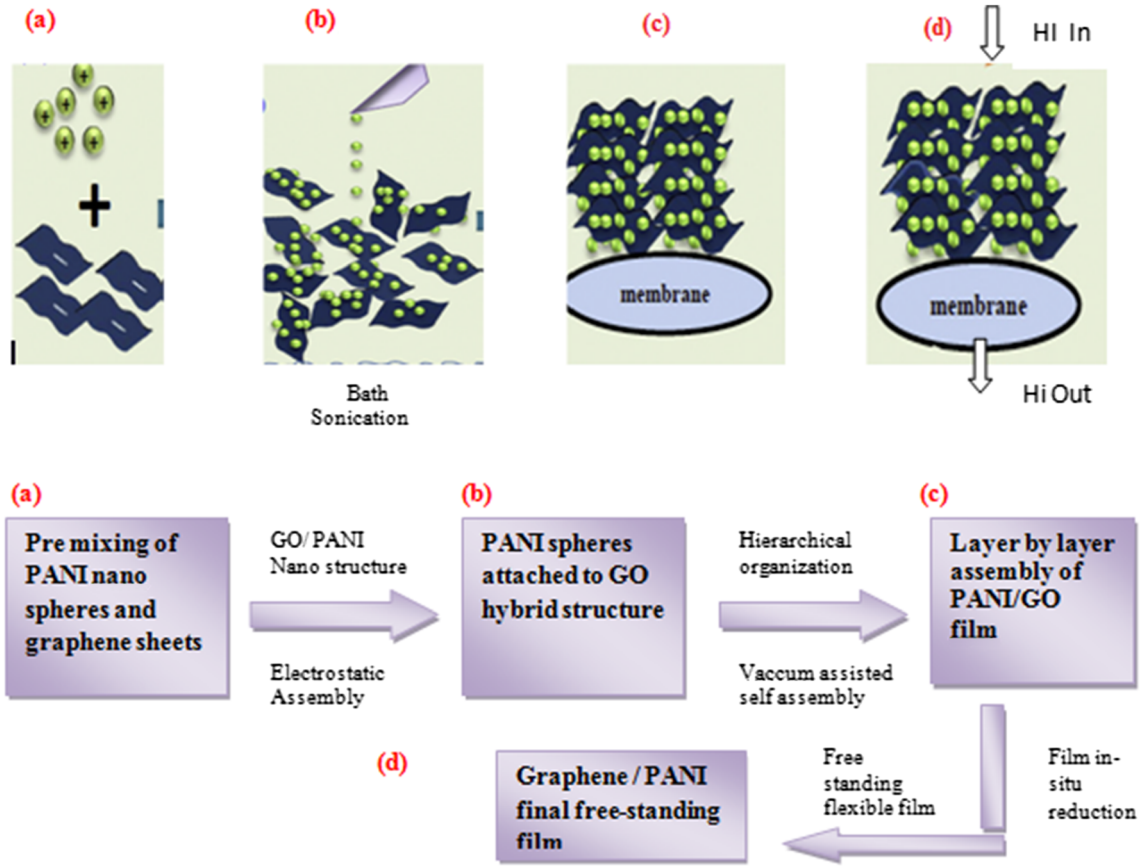

Fig. 2 Schematic representation of steps involved in fabrication of 3D nanocomposites [7]

had optimized the potential applications of CNTs. A large number of metal nanoparticles like Au, Pd, Pt, Fe_3O_4, CdS, SiO_2, and TiO_2 were employed for the coating or the deposition of CNTs using various deposition/coating routes like physiorption, capillary action, solid state reaction, electrodes deposition, and physical evaporation. But, out of all these, only some provided simple and efficient route for coating nanosphere or nanoparticles to CNTs. As per literature, K. R. Reddy et al. [8] have synthesized composites of MWCNTs with Cu_2O_2 nanoparticles using Cu_2SO_4 as precursor using Fehling's reagent in the presence of formaldehyde which acted as the reducing agent. As per their report, the intensity of G and D bands increased thereby eliminating the defect sites while maintaining electronic energy states of MWCNTs in composites.

Among the various transition metal oxides available, $ZnCo_2O_4$ (zinc cobaltite) has emerged as the new horizon for the electrode material for the supercapacitor. It helped in improving the electrochemical performance by boosting the redox reactions which occurred due to the introduction of additional oxidation states. As the morphology of the material plays a vital role in the capacitance enhancement hence, $ZnCo_2O_4$ had been synthesized with numerous structures like nanosheets, nanoparticles, nanorods, and nanowires using different synthesis routes like spray pyrolysis, template synthesis, and facile method. An efficient way for obtaining large capacitance and good catalytic activity, materials with porous structure had extensively been paid more attention by the researches all around the world. In the latest literature, the preparation of mesoporous zinc cobaltite nanosheets was done by using the facile hydrothermal method [9]. The morphology of the sample image obtained by the TEM (transmission electron microscopy) and HRTEM (high-resolution transmission electron microscopy) revealed that the $ZnCo_2O_4$ nanosheets exhibited nearly the hexagonal shape with high surface area of value 191.64m^2/g which was consistent with the SEM images. The specific capacitance of 835 F/g at the current density of 1 A/g was observed. Retention rate of 73.28% for 1000 cycles was maintained under the obtained current density of 8 A/g [9].

Supercapacitors within energy storage systems

Li-ion batteries with the energy densities of nearly 180 watt h/kg (nearly 3–30 times lower than supercapacitors) are the best performers in the area of charge storage. Supercapacitors are the devices which are capable of managing hundred to thousand times more power than the batteries in the same available volume. Hence, supercapacitors are more preferred for the

applications in which energy storage capacity is not much needed whereas the power bursts are required.

Electrolytic capacitors have high power density whereas the batteries are efficient in storing huge amounts of energy but they offer lower power densities (which is less than 1 kw/kg). The Ragone plot for different storage technologies is plotted in Fig.3. The drop in the energy occurring at sufficiently high and low power is due to the presence of internal dissipation and the leakage losses. In this plot, the power densities are marked on the horizontal axes and the energy densities are marked on the vertical axes. The discharge time of the various storage devices is represented by the diagonal lines (E = Pt). As observed from the plot, supercapacitors act as the perfect material to bridge the gap between batteries and the electrolytic capacitors. From the plot, it is clear that the power density of electrolytic capacitors is higher than the supercapacitor (which is nearly 10 kW/kg).

Comparison between battery, capacitor, and supercapacitor

In case of battery, the negative terminal also known as the anode acts as the source of electrons [10, 11]. On connecting the battery with some external circuit, there is movement of ions (electrolyte ions) and thereby allowing chemical reactions to take place. This movement causes the flow of current. If there is any potential difference appearing across the conductors, then in that case, an electric field is developed across the dielectric thereby causing positive charges to accumulate on one plate and negative charges to accumulate on other. In this way, it stores energy. Batteries rely on Faradic reactions taking place in electrode materials itself for charge storage mechanism [2–6]. Supercapacitors store charges through electrostatic charging of electrochemical double layer or through charge transfer via reversible redox reactions. The charge storage mechanism of all the three: battery, capacitor, and supercapacitor is shown in Fig. 4.

A comparative study of supercapacitors with the electrolytic capacitors and batteries is given in Table 1. Since the Ragone plot did not show the comparison of other performance parameters like cost, duty cycle, and safety, hence, the comparison is given. As can be seen, the charging and discharging period of supercapacitors is very short; hence, this serves as a boon for energy recovery systems.

Classification of supercapacitor

Supercapacitors store energy on the basis of the two types of capacitive behaviors: electric double-layer (EDL) capacitance which is obtained from the accumulation of the different electrostatic charges at electrode/electrolyte intersurface and pseudo capacitance which is due to the occurrence of fast and reversible redox processes. Different types of supercapacitors classified on energy storage mechanism along with the electrode materials are given in Fig. 5.

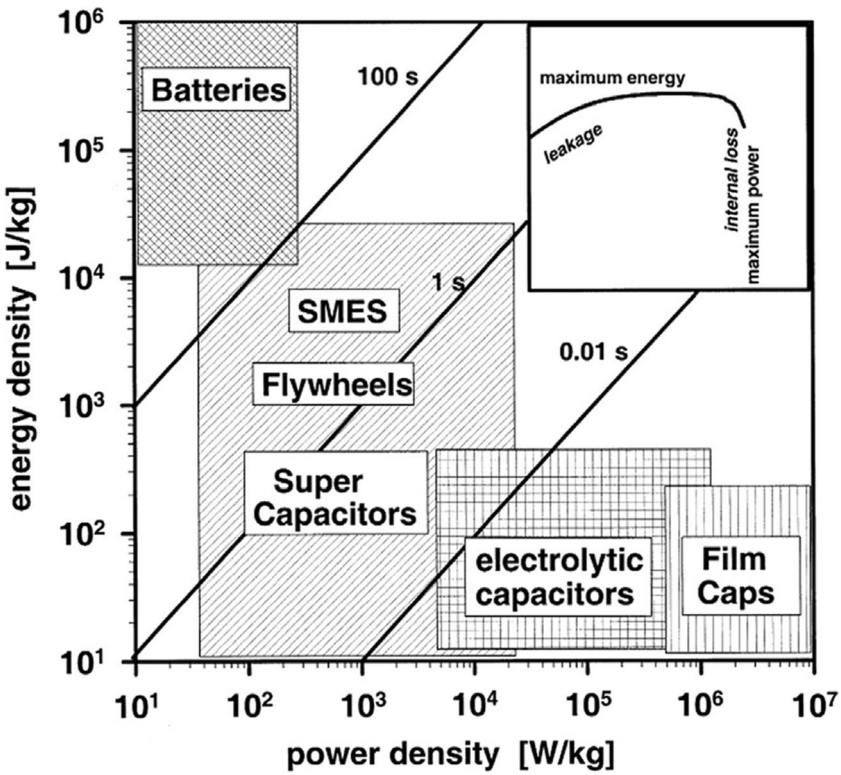

Fig. 3 Ragone plot (energy drop because of leakage losses and internal dissipation)

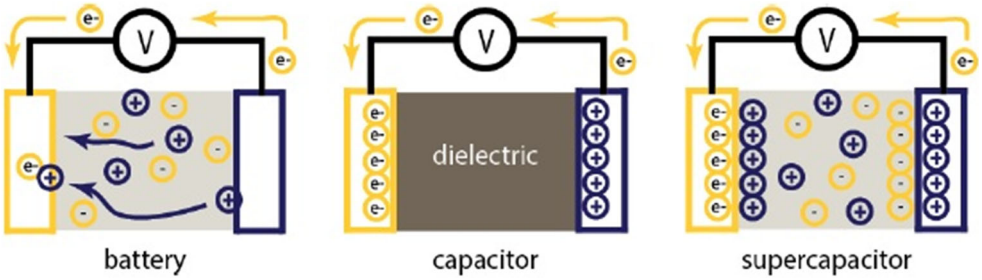

Fig. 4 Charge storage mechanisms by battery, capacitor, and supercapacitor

Though they function together but for the convenience, they are discussed separately.

Electrical double-layer (EDL) in supercapacitor

Fundamental equation of charge storage states that for more charge accumulation requires large surface area which serves as the limitation for conventional capacitors [6–8, 12]. Supercapacitors based on EDL mechanism take the advantage of bigger interfacial area along with the huge charge separation range for storing more charge. An EDL is basically a structure which appears when any charged particle or substance is positioned into the liquid. As theory, the balancing complimentary ions will form on the liquid and their concentration will be more near the surface. There are many theories or different models which are suggested in the literature survey for this interface between a liquid and solid. Some of the models are represented in Fig. 6 and the explanation of each model is also mentioned.

In the given Fig. 6, following notations are being used:

Ψ_o electrode potential
Ψ potential at electrode/electrolyte interface
d Helmholtz distance
IHP inner Helmholtz plane
OHP outer Helmholtz plane

Helmholtz model (1853)

It is the simplest theory which is used for modeling of the spatial charge distribution. The concept of EDL was first introduced and discussed by von Helmholtz in nineteenth century as shown in Fig. 7a, b [13]. The model states that two layers of opposite charges are formed at the electrode-electrolyte interface which is separated by an atomic distance. The charge neutralization takes place by the opposite sign ions which are placed at a distance "d" from the solid [9, 13, 14]. The distance "d" is known as the Helmholtz distance which is the distance from the charged surface to the center of the ion. This model did not provide adequate explanations.

Gouy (1910)—Chapman or diffuse model (1913)

The simple model of Helmholtz was modified by Gouy and Chapman [15, 16]. They considered a continuous distribution of electrolyte ions because of thermal motion in the electrolyte solution. This formed layer was denoted as diffuse layer (Fig. 4b). They suggested equal amount of

Table 1 Comparison between supercapacitor, capacitor, and battery

Parameters	Conventional capacitor	Supercapacitor	Battery (lithium-ion)
Energy storage	W-sec of energy	W-sec of energy	W-h of energy
Charge method	Voltage across terminals	Voltage across terminals	Constant current and constant voltage
Charge time	10^{-3}–10^{-6} s	1–10 s	10–60 min
Cell voltage	6–800 V	2.3 V–2.75 V/cell	1.2 V–4.2 V/cell
Specific energy (Wh/kg)	0.01 to 0.05	1 to 5	8 to 600
Specific power (W/kg)	< 100,000	Up to 10,000	1000–3000
Charge/discharge efficiency	> 0.95	0.85–0.98	0.7–0.85
Cycle life	> 500,000	1 million or 30,000 h	500 and higher
Operating temperature	− 20 to +100 °C	− 40 to +85 °C	− 20 to +65 °C
Form factor	Small to large	Small	Small to large
Lifetime	> 100 k cycles	> 100 k cycles	150 to 1500 cycles
Weight	1 g to 10 kg	1 to 2 g	1 g to > 10 kg

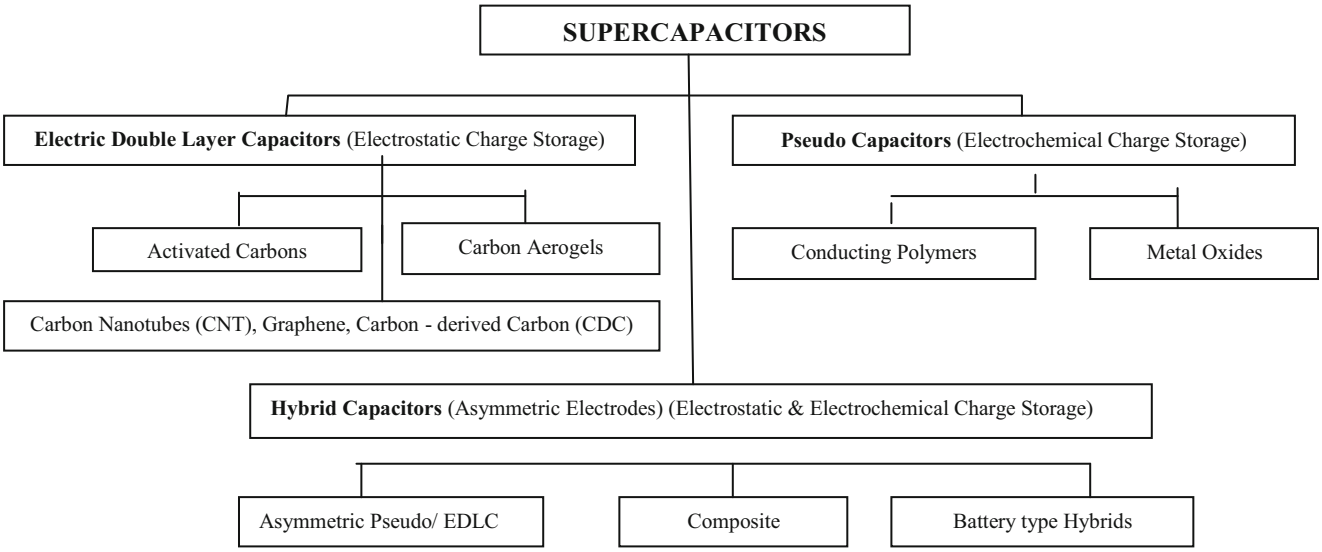

Fig. 5 Taxonomy of supercapacitors along with electrode materials

distribution of opposite ionic charges in the liquid surrounding the charged solid on the constraint that the ions are not attached rigidly to the surface. The diffusion of the ions in the solution is restricted by the counter potential which was set by the ion's departure [17]. The thickness of the diffusion layer was partially determined by the kinetic energy which was possessed by the ions. This model was leading to the over estimation of the EDL capacitance as the capacitance appearing along two different separated charges is inversely proportional to the distance between them. In a condition that if the point charges come close to the electrode surface, then in that case, a very large capacitance value will be obtained. As is observed, the calculated value of the measured thickness is less than the experimental result. Hence, this model fails for double layers which are highly charged [17].

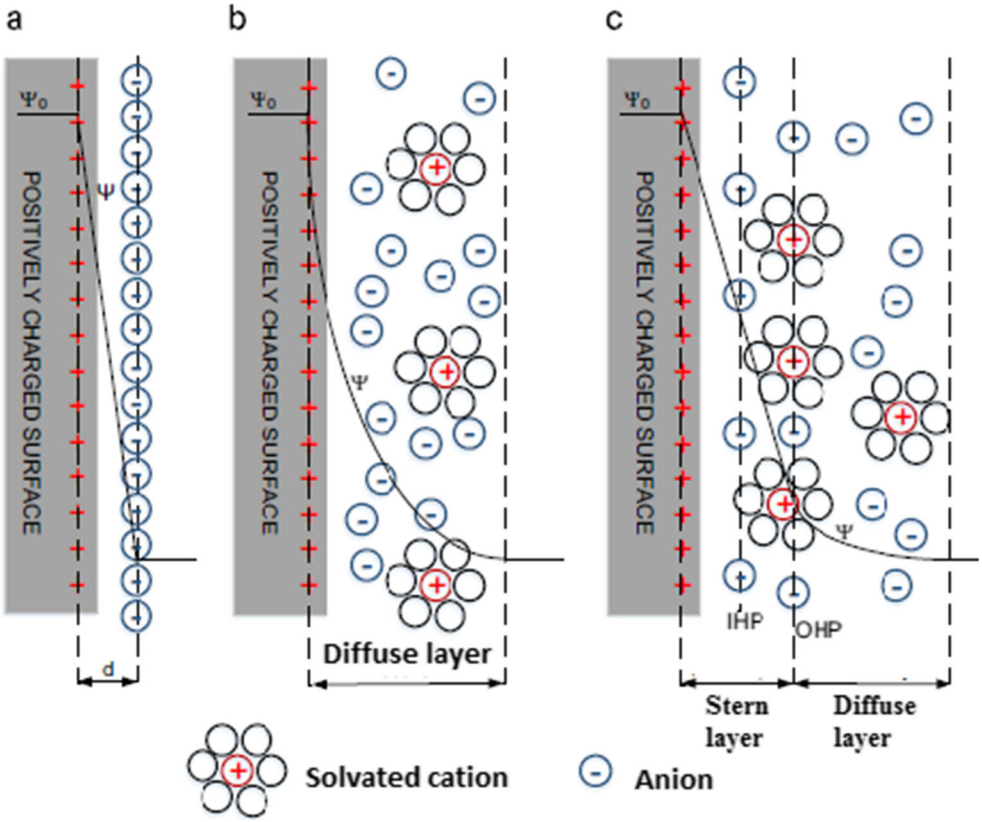

Fig. 6 Models of EDL. **a** Helmholtz Model. **b** Gouy-Chapman model. **c** Stern model showing the different IHP and OHP

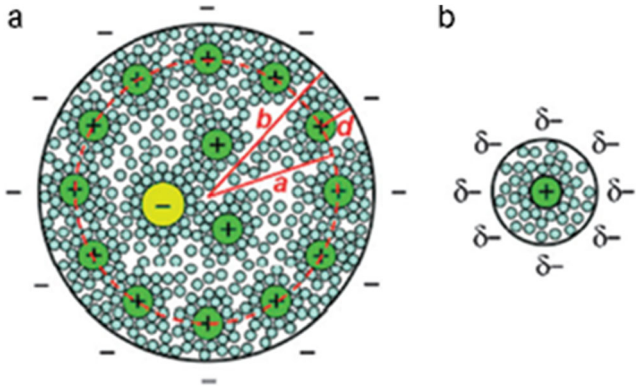

Fig. 7 Schematic diagrams of **a** EDCC model and **b** EWCC model

Stern model or Stern modification of diffuse layer (1924)

Stern combined the model suggested by Helmholtz along with the model given by Gouy-Chapman [18]. He recognized two distinct regions of distribution of ion—inner region was named as compact/Stern layer (e.g., Helmholtz layer) and the outer region known as diffuse layer (e.g., Gouy-Chapman). Gouy-Chapman model was modified by defining that the ions possess finite fixed size thereby providing limitation to their approach to the surface. Compact layer has ions (which are often much hydrated) which are strongly absorbed by electrode; hence, the layer is named so. For distinguishing the different types of adsorbed ions, the IHP (inner Helmholtz plane) and OHP (outer Helmholtz plane) are used. In addition to the hydrated ions, the compact layer has specifically adsorbed ions and the counter-balancing non-specifically absorbed ions [13]. The EDL capacitance (C_{dl}) is given as combination of different capacitances observed from the two distinct regions, namely the capacitance of diffusion region (C_{diff}) and double-layer Stern type of compact layer (C_H):

$$\frac{1}{C_{\mathrm{dl}}} = \frac{1}{C_{\mathrm{diff}}} + \frac{1}{C_H}. \tag{1}$$

where

C_{dl} EDL capacitance
C_{diff} capacitance of diffusion region
C_H capacitance of double-layer Stern type of compact layer

In case of supercapacitor, the electrode is made up of porous material exhibiting high surface area. Here, the EDL behavior at the electrode's pore surface is much more complex than of an infinitely planar surface. The pore size greatly affects the movements of ions into the pore because the pores are too small that in that case they are inaccessible to not contribute to the double-layer capacitance [19].

The specific capacitance (F/g) for each of the electrode for EDL type is assumed to replicate the parallel plate capacitor (given by Frackowiak in 2007) [20] and is given as,

$$C = A\frac{\varepsilon_r \varepsilon_o}{d}. \tag{2}$$

where,

ε_r dielectric constant of electrolyte (dimensionless quantity)
ε_o permittivity of vacuum (F/m)
A specific surface area which is available to electrolyte ions ($m^2\ g^{-1}$)
d EDL effective thickness (m)

As per the above equation, there exists a linear relation between the capacitance and specific surface area. However, experimentally, this simple relation does not hold in many cases [20–23]. Various literature survey studies suggested that pore sizes below 0.5 nm are not easily reached to the hydrated ions [23, 24]. Pore sizes of dimension smaller than 1 nm are too small to be accessible by the organic electrolytes [25]. EDL can be formed in micropores if partial desolvation of hydrated ions occurs. A significant increase in capacitance for carbon electrodes was observed by Gogotsi and his co-workers. Their further investigation suggested a maximum capacitance value when pore size of the electrode was comparable to that of the size of ion. These observations thereby confirmed that the capacitance contributions from the pores of sizes were smaller than that of the size of solvated ion. These discussions and findings were not as relevant as both the diffuse and the compact layer cannot be easily accommodated in such limited spaces of micropores.

The addition of mesopores in small amounts onto micropore surface increases the power handling capability of ultracapacitors. For describing the capacitive behavior in case of nanoporous carbon-based supercapacitors, a heuristic approach was suggested by Huang and co-workers in 2008 [26, 27]. They suggested capacitive mechanisms for the electrodes with different pore sizes and they considered pore curvature for their analysis. The two different models are explained and shown in Fig. 7.

EDCC (electric double-cylinder capacitor) model

This model was used for mesoporous carbon electrodes with cylindrical pores. If the pore sizes are large enough so that the pore curvature becomes insignificant, then in that case, the EDCC model goes back to the traditional planar model. The capacitance estimation is given as [28].

$$C = A\frac{\varepsilon_r \varepsilon_o}{b\ln\left(\frac{b}{b-d}\right)} \tag{3}$$

EWCC (electric wire-in-cylindrical capacitor) model

The microporous carbon electrodes were modeled with the help of this model. The ions in case of being microporous line up in the center of the cylindrical pore and hence the value of capacitance is calculated as

$$C = A\frac{\varepsilon_r\varepsilon_o}{b\ln\left(\frac{b}{a_o}\right)} \tag{4}$$

where,

a_o effective ion size
b pore radius
d distance between approaching ion and the carbon electrode

Dielectric constant can be calculated using Eq. 4 from the fitting results, which was very close to the vacuumed valve. This indicated that the hydrated ions were fully dissolved before entering the micropores. Since, in more realistic approximation, the shape of the pore in carbons is assumed to be slit rather cylinder; hence, a different sandwich-model was deduced and it was represented as [29]

$$\frac{C}{2A} = \frac{C_s}{A} = \frac{\varepsilon_r\varepsilon_o}{b-a_o} \tag{5}$$

Carbon electrode materials

The explanation of the most important materials for electrodes is presented in this section of the paper [30, 31]. The carbon materials are discussed thoroughly along with some new materials available. In today's nanoscale regime, the importance of nanotechnology is becoming many folds as it is finding wide application areas like sensors, computing, and biomedical. Because of their low cost and high availability, carbon-based electrode materials are the most widely used electrode materials. This section provides research developments in these materials from most widespread types to the recent advancements. Figure 8 shows the rectangular cyclic voltammogram for the different carbon-based materials in both types of organic and aqueous electrolytes.

Graphene

Graphene is a well-known one-atom thick sheet, 2-D mono layers composed of all-sp^2 hybridized carbon atoms in a poly-aromatic crystal lattice of honeycomb structure. It possesses some of the most intriguing properties like high surface to volume ratio, good thermal and electrical conductivity, structural flexibility, highly tunable surface area (up to 2675 $m^2\ g^{-1}$), short diffusion distance (due to its thickness), good chemical stability, strong mechanical strength (~ 1Tpa), and wide potential window [32–36]. Apart from these, it also takes the advantage of having large surface area of monolayer (theoretically 2620 $m^2\ g^{-1}$) and open pore system which helps in improving the transport kinetics phenomenon.

Due to its improved capacity, rate, and cycle capability and excellent physiochemical properties, these materials are preferred for high-performance electronics, electrochemical energy storage systems, and sustainable energy generation devices [37–49]. A traditional way of obtaining graphene is shown in Fig. 9, in which the graphite is initially oxidized to produce graphite oxide. This is achieved using Hummer's method [50] or modified Hummer's method [51]. For producing GO sheets, complete exfoliation of graphite oxide can be done using simple sonication [52]. Reducing GO with hydrazine solution or any other reducing agent provides chemically derived graphene.

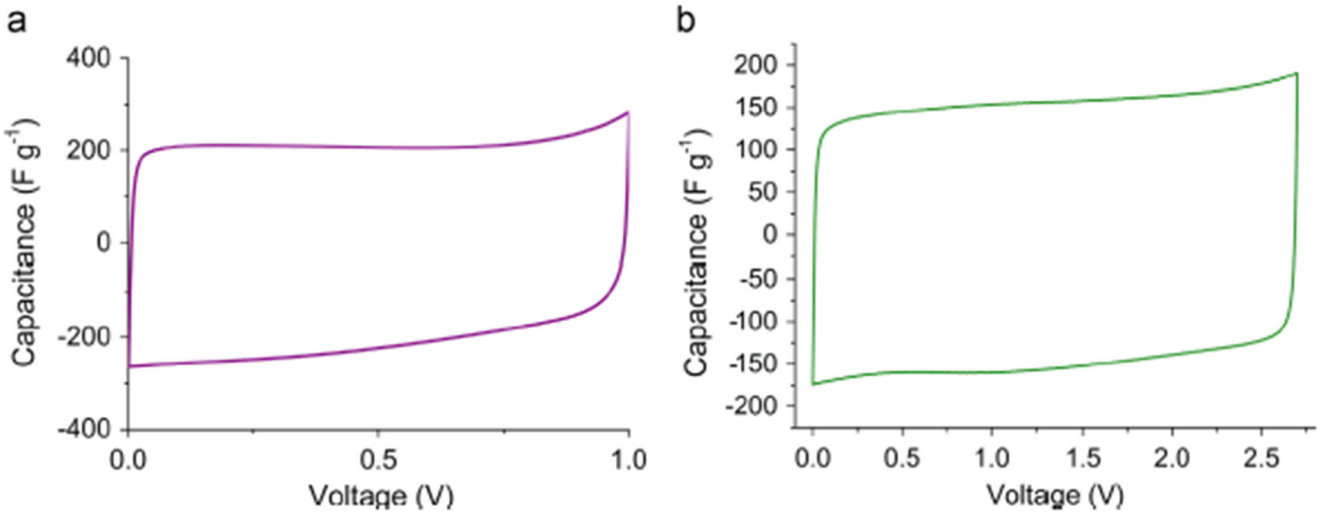

Fig. 8 Cyclic voltammogram of EDLC cell at 5 mVs^{-1} in **a** aqueous 6MKOH and **b** organic tetraethylammonim tetrafluroorate electrolytes

Fig. 9 Chemical route to synthesis of chemically derived graphene

Graphene-based supercapacitors with ionic liquid electrolytes were reported with energy density of value 31.9 Wh kg^{-1} and specific capacitance of 75 F g^{-1}. They were also reported with organic and aqueous electrolyte having specific capacitance of 99 F g^{-1} and 135 F g^{-1} respectively. Reduced graphene exhibiting low agglomeration showed a maximum specific capacitance of 205 F g^{-1} and energy density of 28.5 Wh kg^{-1} in aqueous electrolyte.

Graphene sheets exhibit the drawback of easily forming irreversible agglomerates and restacking to their graphite structure. Hence, the determination of intrinsic capacitance becomes very difficult. As per the literature survey, the intrinsic capacitance of the EDL in graphene was reported to be 21 μ F m^{-1} [32]. The interfacial capacitance was calculated from the surface area which was dependent on the number of layers. For graphene-based supercapacitors capable of operating till 4.5 V, an energy density of 85.6 Wh kg^{-1} at room temperature and 136 Wh kg^{-1} at 80 °C in ionic liquids was reported back in the literature. Due to its restacking issue, the graphene suffers from the problem of irreversible capacity loss which in term also reduces the initial columbic efficiency. This re-stacking problem arises due to the presence of Vander wall interactions between the adjacent sheets which reduces its energy density as a consequence of reduction of the surface area.

To avoid this restacking problem, the hybridization of graphene with porous carbon, carbon nanotubes (CNTs), and carbon nanofibres (CNFs) has emerged as a good solution. Graphene nanoribbon (GNR/C) composite nanofibers were developed using electro spinning from polyacrylonitrile (PAN)-containing GO nanoribbons (GONRs) followed by successive twisting and carbonization [53]. PAN-containing GONR nanocomposites were highly oriented during their electro spinning, and by carbonization method also had been converted to all-C materials GNR/CNF [54].

Graphene can be synthesized using several methods. For small scale, production "scotch tape" method is most widely used. For research purposes, other synthesis routes like CVD, arc discharge, exfoliation, unzipping of CNT, chemical synthesis, molecular beam epitaxy, electrically assisted synthesis, solvothermal, pyrolysis, and epitaxial growth are preferred. The obtained graphene layer is transferred either to any medium or substrate for the formation of composites. For the generation of 2D graphene, silicon carbide wafers are thermally treated.

Oxides of graphene serve as an important alternate material to be used for nanocomposite formation. Humer's method can be used for the synthesis of oxide of graphene which requires de-ionized water along with permagnate concentrated acid (e.g., H_2SO_4), graphitic flakes, and nitrates (e.g., sodium nitrate). Metal oxide (in nanocomposite form) is the next important component in the graphene oxide nanocomposite. Metal-organic precursor in suitable basic or acidic pH conditions is used to prepare metal oxide in excellent yield with a good controlled size.

Metallic powders have also been used for the preparation of oxide nanoparticles. For example, for the sysnthesis of zinc oxide at room temperature, metallic zinc powder acts as the source precursor in the alkaline medium (KOH). In this method, the metal hydroxide releases its water to form very fine oxide nanoparticles. When the graphene sheets are immersed in the solution, oxide-based graphene nanocomposites are developed by depositing the oxide nanoparticles on the graphene. The proper selection of oxide is an important factor for the consideration in the synthesis of oxide-based graphene nanocomposites. Since the oxides are gas sensitive materials, hence, they are not suitable for sensing because of lack of surface active sites and high resistivity. These factors lead to the conclusion that for the synthesis of oxides and their resulting composites, the optimization of process parameters is very important. Hydrothermal is a common route for the development of graphene oxide nanocomposites.

Clay plays an important role in the formation of nanocomposites by intercalating them between the graphene oxide layers. Various other techniques like mechanochemical intercalation and solvothermal have been suggested for synthesizing composites of graphene with silica and zinc oxide respectively. Self assembly is also very successful technique for developing graphene oxide nanocomposites. For developing graphene TiO2 nanocomposites or graphite oxide TiO_2 nanocomposites, the solvent exfoliation or in situ growth of TiO2 nanoparticles on graphene oxide nanosheets followed by annealing process at 200 °C have been reported in the literature. Facile hydrothermal synthesis route was used to develop

nanocomposites using tin oxide and reduced graphene oxide nanoparticles.

Different capacitance values were obtained for graphene-based supercapacitor in early literature. For supercapacitors with ionic liquid electrolyte energy density of 31.9 Wh kg^{-1} and capacitance (specific) of 75 F g^{-1} was reported [55]. In aqueous electrolyte, specific capacitance of 135 F g^{-1} was observed whereas in organic electrolyte, specific capacitance of value 99 F g^{-1} was reported [56]. In aqueous electrolyte, the reduced graphene with low agglomeration achieved an energy density of 28.5 Wh kg^{-1} and a specific capacitance of 205 F g^{-1} [57].

For the formation of 2D and 3D macroscopic structures, graphene-based CNTs and CNFs materials have been employed [58]. The energy density of 65.1 Wh kg^{-1} and 82.4 Wh kg^{-1} at 650 Wh kg^{-1} was reported lastly using exfoliated graphene with anchored polypyrrole [59]. The specific capacitance of 143.6 F g^{-1} was obtained by graphene nanosheets-tungsten oxide composite [60], and specific capacitance of 479 F g^{-1} was reported by RuO_2 graphene hybrid material [61].

Another important method of improving electrochemical properties of graphene-based electrodes is to dope graphene with chemicals having electron donors and acceptors. As per the reports from the literature, a specific capacitance of 242 F g^{-1} was achieved using N-doped-graphene oxide supercapacitor and capacitance of 320 F g^{-1} was obtained for highly nitrogenated graphene oxide [60, 62, 63].

A 3D framework structure consisting of polyanniline and graphene nanosheets was prepared. As compared to specific capacitance of 190.6 F g^{-1} for pure GNs, this structure provided a high specific capacitance of 261.4 F g^{-1} for the current density of 100 mA g^{-1} was obtained [64]. An asymmetric pseudo capacitor was obtained by assembling graphene/CNT-PANI with graphene/CNT electrode. The obtained maximum energy and power density were 188.4 Wh kg^{-1} and 200.5 kW kg^{-1} respectively. The charging voltage was up to 4 V. The capacitance value dropped 18% after 1000 cycles that indicated a good cycle of the designed electrodes [65]. Fe_2O_3-graphene nanocomposites were synthesized using hydrothermal method. The specific capacitance of 226 F g^{-1} at a current density of 1 A g^{-1} was obtained for Fe_2O_3-RGO nanocomposite electrodes [66].

Various natural sources like rice husk, jute, and sugar were used to synthesize different graphene-like nanostructure. It was observed that activated carbon nanostructures possessed higher specific capacitance of value 476 F/g in comparison to non-activated carbon. Various characterization techniques like FTIR, Raman Spectroscopy, and SEM were used for the characterization of different nanostructures [67].

In the past few years, graphene oxide has emerged as a promising building block for the fabrication of various functional graphene-based nanomaterials. To date, a large number of reports have been about zinc oxide nanostructure 1D graphene composites with wide applications as sensors, photovoltaic degradation, and Li-ion batteries. Due to its small size synergistic interaction and surface effect, the immobilization of nanostructures on the graphene surface has attracted much attention. Mouss et al. have reported the preparation of zinc oxide rods/rGO composites for sunlight-driven photocatalysis with the help of solvothermal reaction. Authors Zhao et al. had prepared zinc oxide-nanorods/graphene nanostructures as a glucose binder, but the multi-step process or designed linkers introduction had limited its application.

Few works in the literature had been reported for the facile synthesis of zinc oxide nano rods/rGO composites with excellent performance and well-defined morphology for further photocatalysis application. Some researchers have reported a convenient route to in situ synthesize zinc oxide nanorods/rGO composites using graphene oxide sheets, hexamethylenetetramine (HMT), and zinc acetate ($Zn(CH_3COO)_2$) as precursor through the green and facile hydrothermal route in one pot synthesis method. During the process, graphene oxide sheets were reduced to rGO sheets. The zinc oxide nanorods with diameter in the range of 100–200 nm and length of 1–2 μm were formed and were uniformly distributed over the entire surface of rGO sheets. The synthesized nanocomposites possessed enhanced photo catalytic activity compared with pure zinc oxide powders. Though the synthesis route developed was economical and environment friendly but the nature of the photo catalytic property was elaborated specifically.

In a report [12], nanostructured CB-PANI composite was synthesized as shown in Fig. 10. This was carried out through p-TSA micelle-assisted synthesis route which used an in situ self organization process. Various electrical, thermal, structural, and morphological properties were investigated using four-probe meter data, TGA, FT-IR, UV-Vis, FESEM, and XRD. The mass fraction of CB increment from 5 to 23% improved the nanocomposite's thermal stability due to the π-π interactions between the aromatic rings of CB and the PANI. The resultant CB-PANI composites formed various structures via self-organization process and showed good electrical conductivity of value 1.38 S/cm which is approximately three times greater than that of the pristine PANI. As per the results, the morphology of the resulting nanocomposites was greatly affected by the concentration of the carbon black.

For acquiring good super capacitive performance, graphene nanosheets were prepared at 673-K thermal exfoliation temperature. The specific capacitance of 233.1 F g^{-1} was obtained in 6 mol L^{-1} of KOH electrolyte [68]. Sandwich-like nitrogen-enriched porous C/graphene composites were manufactured by carbonization of PAN nanofiber papers [67]. The activation was carried in 6 M of KOH (aqueous electrolyte) at high temperature. High specific area in the range of 1957.2 to 2631.8 m^2 g^{-1} was exhibited by the

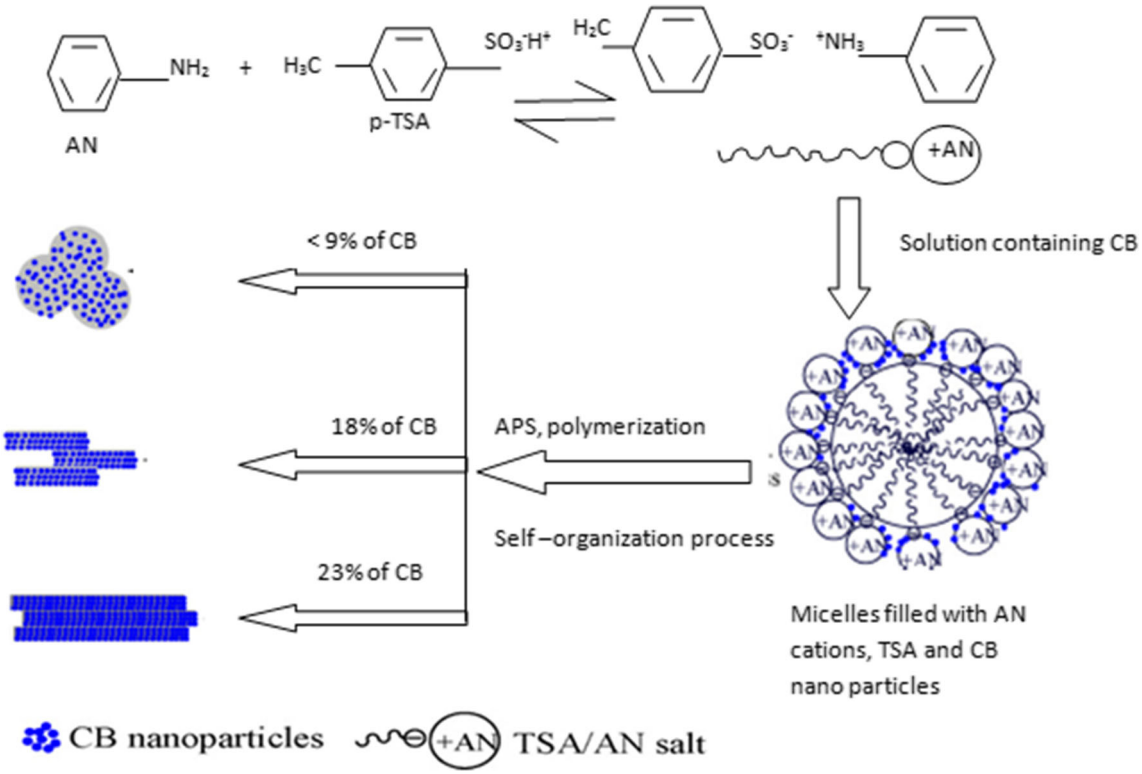

Fig. 10 Schematic diagram representing the formation of CB–PANI nanocomposites [12]

composites. A high specific capacitance of value 381.6 F g^{-1} at current density of 0.1 A g^{-1} was achieved. The assembled aqueous symmetric supercapacitor delivered high energy density of 13.2 Wh kg^{-1} at power density of 25.0 W kg^{-1} and 8.3 Wh kg^{-1} at 4.7 kW kg^{-1} with 62.9% of retention rate [67]. Table 2 gives the summary of the supercapacitors performance parameters based on graphene electrodes.

In previous literature, formation of radicals on surface of g-CN was performed using co-catalyst. In their paper, the authors have investigated a facile route for the formation of photo catalytically active hydrocarbons-reinforced hydrogels without having any type of co-catalyst. For performing the photo-induced g-CN functionalization, one-pot visible light-induced grafting method was suggested for integrating the allyl compounds onto the surface of g-CN [86]. As compared to the unfunctionalized g-CN, increased dispersion stability (up to 10% in aqueous and 2% in organic) was observed along with low sonication times for redispersing g-CN.

Some of the authors have worked on implementing graphite oxides as effective fine retardants of epoxy resin. Their experiment results have shown that graphene oxide (GO) on proper oxidization manifested optimum fire retardant properties. An enhanced fine dispersion of GOs in epoxy resin was obtained using sonication which also reduced the fire retardant effects of GO [87]. The morphology of cryogenically fractured surface of M_2O_5 was clearly observed by SEM which showed the homogeneous dispersion of GO in epoxy resin with particle size of μm or even less.

In a study, the compatibility of TRG (thermally reduced graphene) with multi block co polyester elastomer (PEE) comprising of PBT (poly butylenes terephthalate) segments and poly tetramethylene ether glycol segments was carried out in detail by examining the electrical conductivity, tensile properties, and the morphology of TRG polyester composites. Few researchers in their report have suggested a method in which they analyzed the quantitative compatibility of graphene with polymers using Hansen solubility parameters (HSP) [88]. The authors have also analyzed the compatibility of TRG with some random co-polymers of ethylene like poly (ethylene-co-acrylic acid EAA) and poly (ethylene-co-vinyl acetate EVA) using the HSP. The morphology observed by SEM and TEM (optical) microscopy showed that the size and number of large aggregates of graphene layer was reduced as the contents of PTMG (poly (tetramethylene ether) glycol) segments in the polyester was reduced. This was due to the enhanced compatibility of polyester with TRG. This result suggested that the TRG in comparison to PTMG segment with non-aromatic structure and lower polarity was more compatible with PBT segment possessing aromatic structure and high polarity. As an evident result, finer dispersion of TRG in the polyester matrix and good adhesion at the TRG/polyester interface were observed in the SEM and optical microscopy. It was also observed that on increasing the content of electrically conductive filler in polymer matrix, the electrical conductivity value of the composite increased. Negative results were obtained for the tensile strength parameter. The molecular strength and orientation of

Table 2 Overview of performance parameters of graphene-based electrode materials

Electrode material	Specific capacitance (F g^{-1})	Energy density (ED) (Wh kg^{-1}) and power density (PD) (kW kg^{-1})	Specific surface area (m^2 g^{-1})	Growth process, morphology, cycle stability, and other parameters	Electrolyte used, potential window, and scan rate (SR)	Ref.
Graphene PTFE binder*	• KOH – 40 mV/s – observed capacitance is 116 (0.1–0.9 V) • Organic electrolyte AN- 20 mV/s observed capacitance is 100 (1.5-0 V) • Organic electrolyte using PC – 20 mV/s- observed capacitance is 95 (2–0 V)	–	• Two electrode cell configuration • SSA - 705	• Growth process-Humers method suspending graphene oxide sheets in water and then reducing them using hydrazine hydrate • CV was nearly rectangular • Conductivity - (~ 2 × 102 S/m)	• KOH (1 V) PC (2.7 V) AN (2.5) • SR - 20 mV/s – 400 mV/s	[69]
Exfoliated graphene	• Aqueous (H_2SO_4) – EG –cap. 117 at 100 mV/s • (EG – cap. 100 at 1000 mV/s • DG – 35 • CG – 6) • Ionic liquid – 75	31.9/ -	• For EG – 925 (exfoliation of graphitic oxide) • For DG – 520 (transformation of nano diamond) • For CG (Camphor)- 46 • EG - 12·4 μF/cm^2 • DG – 6.7 μF/cm^2	• Thermal exfoliation of graphitic oxide • Heating nanodiamond at 1650 °C in a helium atmosphere • Decomposition of camphor over nickel nanoparticles	• 1 M H_2SO_4 (1 V) electrolyte, for ionic electrolyte $PYR_{14}TFSI$ up to 3.5 V • SR- 100–1000 mV/s	[70]
Graphene	• 205 • specific capacitance per surface unit - 64 μF cm^{-2}	28.5, 10	320	• Modified Humers method, • constant current density of 100 mA/g • ESR value (3.2 Ω)	• KOH aqueous electrolyte • SR of 0–1 V • Cell voltage of 1 V	[57]
RuO_2/GNS	• For GPCP- 900 s-gravimetric capacitance - 233 F and volumetric capacitance - 135 F cm^{-3} • For G paper - gravimetric capacitance – 147 volumetric capacitance - 64	20.1, 10	• For G paper- 94 • For GPCP 900 s - 39	• In situ anodic electro polymerization of polyanniline film on graphene paper	• ~ 97.9% sp. cap. remaining after 1000 cycles, • redox reaction resistance of G paper– 2.72 Ω • ESR of the GPCP (0.36_0.51 Ω) • SR – 2–20 mV/s	[71]
Graphene water as spacer	• For CCG - 215 273.1 • 156.5 when the SC is operated at an ultrafast charge/discharge rate of 1080 A g^{-1}	• 150.9/776.8 • The SSG film can provide a maximum power density of 414.0 kW/kg	–	• Filtration technique • It can retain over 97% of capacitance over 10,000 cycles	• H_2SO_4 electrolyte (1 V) • Potential window till 4 V • SR – 2–10 V/s	[72]
Pristine graphene	• For G (pristine graphene) – 80 μ F cm^{-2} • For RMGO (reduced multilayer graphene oxide) – 390 μ F cm^{-2} • For stacked – 140 μ F cm^{-2}	–	• 1310 – specific area of one side of graphene	• For G – CVD For RMGO – LBL (layer by layer) assembly • Flat morphology of graphene • Stable at charge/discharge for 1500 cycles • Constant current density of 176 mA g^{-1}	• PVA-H_3PO_4 polymer gel electrolyte • SR – 1–100 mV/s	[73]
Graphene sheet by laser irradiation	• Areal capacitance of the LSG-EC was calculated to be 3.67 m F/cm^2 and 4.04 m F/cm^2 in 1.0 M H_2SO_4	1.36 mWh/cm^3/~ 20 W/cm^3	1520	• Laser-scribed graphene-based electrochemical capacitors • retains > 96.5% of its initial response after 10,000 cycles • Conductivity -(1738 S/m)	• 1 M H_3PO_4 electrolyte • SR 100–10,000 mV/s • Potential window up to 3 V • Retention of 96.5% of its initial capacitance after 10,000 cycles	[74]
Graphene sphere	• 174 at current density of 8.4 A g^{-1}	• Gravimetric energy density - 174 • Gravimetric energy density- 338	3290	• Chemical activation of graphene-based hollow carbon spheres. • Crumbled morphology for GO particles in size from 1 to 4 μm diameter • Smooth and flat surfaces morphology for 3 to 10 μm diameter • ~ 94% capacitance retention over 1000 cycles • ESR of 5.7 Ω	• Ionic electrolytes like [EMMI][TFSI] and [BMIM][BF4], in acetonitrile • two-electrode symmetrical cell configuration • Potential window (0–3.5 V) • SR - 100–400 mV/s	[75]
Graphene sheet thermally reduced in water + Gel as spacer	• Volumetric capacitance – *65 F/cm^3* • Gravimetric capacitance- 156	17.5, –	2000 • Effective density of the active electrode material - *0.46 g/cm^2*	• Dispersion of graphene oxide in water, followed by the addition of *$EMImBF_4$*. In –situ thermal reduction • Retention over 90% of their maximum capacitance • RS drops from 33 to 10 as the reduction temperature is increased from 270 to 340 °C	• Ionic liquid $EMImBF_4$ (4 V) • SR – 500 mV/s • Potential window – (0–3.5 V)	[76]
Exfoliation of graphite in aqueous organic salt	• Area capacitance of the flexible EG paper SC - ~ 11.3 m F cm^{-2} • Gravimetric capacitance - 18.8 to 56.6		11.3 m F cm^{-2}	• Electrochemical exfoliation of graphene sheets into aqueous solutions of different inorganic salts • After 5 s, the edge of the graphite foil expanded, and the cracks in the graphite layers increased and afterwards they were dispersed into the electrolyte solution	• Rate capability of 5000 mV/s • Low oxidation degree (a C/O ratio of 17.2), • hole mobility of 310 cm^2 V^{-1} s^{-1}	[77]
Nitrogen-enriched porous C/graphene composites	381.6	• ED of 13.2 Wh kg^{-1} at a PD of 25.0 W kg^{-1} • ED of 8.3 Wh kg^{-1} at PD of 4.7 W kg^{-1} with retention rate of 62.9%	1957.2 to 2631.8 2896.4 m^2 g^{-1} for N-ACF@Gr1 1957.2 m^2 g^{-1} for N-ACGrF@Gr1	Modified Hummers method N-ACF@Gr1 has conjugated bubble-like structure, while N-ACGrF@Gr1 demonstrates crumpled graphene surface with	6 M KOH electrolyte SR up to 200 mV/s current density of 0.1 A g–1	[67]

Table 2 (continued)

Electrode material	Specific capacitance (F g^{-1})	Energy density (ED) (Wh kg^{-1}) and power density (PD) (kW kg^{-1})	Specific surface area (m^2 g^{-1})	Growth process, morphology, cycle stability, and other parameters	Electrolyte used, potential window, and scan rate (SR)	Ref.
				the underneath revealing a framework of nanofibers		
3D electrochemically reduced graphene oxide pErGO@Cuf/Cu wire	• Specific capacitance- 81 ± 3 •Area specific capacitance of 283.5 m F cm^{-2} • Length-specific • Capacitance of 40.5 m F cm^{-1}	• Energy density: • 11.25 Wh Kg^{-1} • 5.6 μWh cm^{-1} • 39.3 μWh cm^{-2} • Power density-5 kW Kg^{-1} • 2.5 mW cm^{-1} • 17.6 mW cm^{-2}		• In situ growth • Pores distributed symmetrically • average size of 40 μm	• 94.5% • Csp retained even after 5000 cycles at 5 A g^{-1} • − 0.95 V – (− 1.2 V) • SR - 0.01 V/s – 100 V/s • Current densities from 0.5 to 10 A g^{-1}	[78]
Bendable graphene@iron oxide hybrid film (GFeF) electrode	• Gravimetric capacity - 855.2 mA h g^{-1} at 0.02 A g^{-1} • Volumetric capacity −1949.9 mAh cm^{-3} at 0.02 A g^{-1}	• Energy density 129.6 Wh kg^{-1} • Power density 1870 W kg^{-1}	• Surface area - 375 m^2/g • Average size of mesopores and micro pores was around 33.2 nm	• Extended filtration-assisted self-assembly growth method • 93% capacitance retention after 500 cycles • conductivity of GOFeF - 0.5 Sm^{-1} while for GFeF-2264 Sm^{-1}	• Potential −3.5 V • SR - 2 mV s^{-1} • Electrolyte - Li + containing organic solvent	[79]
Transition metal oxide nanorods/ reduced-graphene oxide (rGO) hybrid fibers MnO_2 nanorods/rGO hybrid fiber as positive electrode, MoO_3 nanorods/rGO hybrid fiber as negative electrode	• For MnO_2/rGO hybrid fiber-281.3 F cm^{-3} at 2 mV s^{-1} • and 135.1 F cm^{-3} at 100 mV/s • Volumetric capacitance – 53.5 F m^{-3} • at a current density of 100 mA cm^{-3}	• Energy density - 18.2 mWh cm^{-3} •Power density - 76.4 mW cm^{-3}	• Surface area- 130.5 m^2 g^{-1} • Pore size ranging from 2.5 to 50 nm	• Wet-spinning growth method • Within hybrid fiber, rGO layers interconnected and • aligned along axial direction • rGO sheets were • well-separated and formed porous structure • Capacitance retention rate – 96.6% after 5000 cycles	• Electrolyte - H_3PO_4/poly (vinyl alcohol) (PVA) • Potential - 1.6 V • SR – 5 - 100 mV/s	[80]
Hierarchically ordered mesoporous carbon/ graphene (OMC/G) composites	• OMC/G composites- 329.5 F/g • OMC-234.2 F/g • OMC with graphene - 217.7 F/g at a current • density of 0.5 A/g		• Surface area- 2109.2 m^2/g (after KOH activation) • 1474.6 m^2/g after OMC activation	• Solvent-evaporation-induced self-assembly (EISA) • method • large domains of ordered stripe-like and hexagonally arrays of mesopores • 96% after 5000 cycles at a current density of 10 A/g	• Electrolyte- 6 M KOH • SR - 2 mV/s	[81]
MnO_2 on hierarchical porous carbon nanofiber/ graphene (MnO_2/HPCNF/G)	• 210 F g^{-1} at a current density of 1 mA cm^{-2})	• Energy density (24–19 Wh kg^{-1} • Power densities ranging from 400 to 10,000 W kg^{-1}	*• 487 m2 g^{-1} for MnO_2/HPCNF/G(0) 658 m^2 g^{-1} for MnO_2/HPCNF/G(3)* *• 699 m^2 g^{-1} for MnO_2/HPCNF/G(5)*	• One-step electrospinning and thermal growth process long and continuous cylindrical morphologies, interconnected structure • For MnO_2/HPCNF/G(0) average diameter: • 375–25 nm current density range: 1–20 mA cm^{-2} • For MnO_2/ HPCNF/G in average diam. About 575–25 nm • Rough surfaces with small NPs and needle-like particles on NFs surface	• Electrolyte: 6 M KOH aqueous • Potential range 0.2–0.8 V • SR 10 to 100 mVs^{-1} • 170 F g^{-1} retained at a high current density of 20 mA cm^{-2} • *electrical conductivity: 0.67 Scm^{-1} for MnO_2/HPCNF/G(0)* • *0.79 Scm^{-1} for MnO_2/ HPCNF/G(3)* • *0.79 Scm^{-1} for MnO_2/HPCNF/G(5)* • *0.76 $Scm^{-1}$for MnO_2/HPCNF/G(7)* • 95.7% after 1000 cycles	[82]
Layered barium transition metal fluorides, $BaMF_4$ (M ¼ Mn, Co, Ni)	• Specific capacity: • For $BaCoF_4$ • 15.4 mAh g^{-1} at • 0.8 A g–1 • For $BaMnF_4$ 30 mA h g^{-1} at 0.5 A g^{-1} • For $BaNiF_4$ 12.3 mA h g^{-1} at 0.4 A g^{-1} • SC's value: 360 F g–1 for $BaCoF_4$ • for $BaNiF_4$ 200 F g^{-1} • 150 F g^{-1} for $BaNiF_4$	–	*• Density of $BaMF_4$ electrodes are 0.13 g cm^{-3}, 0.18 g cm^{-3}, and 0.15 g cm^{-3} respectively for $BaCoF_4$, $BaMnF_4$, and $BaNiF_4$ respectively*	• Hydrothermal growth method • Morphology: sheet structure, lateral size (order of 10 μm) • Three-electrode configuration • ESR values: • $BaCoF_4$–0.8 Ω • $BaMnF_4$–1.4 Ω $BaNiF_4$–3.6 Ω	• Energy efficiencies • 61% - ($BaMnF_4$) • 63% - ($BaCoF_4$) 55% - ($BaNiF_4$) after 1000 cycles • Voltage range is −0.2 to 0.3 V • SR 10 to 60 mV s^{-1}	[83]
3D CoO quantum dots/ graphene hydrogels	• 889.7~822 F g^{-1} at current densities of 2 to 50 A g^{-1}	• Energy density of 28.7 and 23.0 Wh kg^{-1} at a power density of 1600 and 12,000 W kg^{-1}	• For hybrid aerogels141.2 m^2 g^{-1} • average pore diameter - 12.23 nm, • *pore volume - - 0.43 cm^3 g^{-1}* • For pure freeze-dried GS hydrogels, • SSA: 393 m^2 g^{-1} • pore volume - 0.27 cm^3 g^{-1} average pore diameter - 2.7 nm	• Modified Hummers method Capacitance retention as high as 92.4%. after 5000 cycles • Uniform distribution of CoO quantum dots size 3~6 nm on surface of graphene	• Electrolyte: 2 M KOH • 2 to 50 mV s^{-1} • 0–0.55 V	[84]
Graphene nanowalls (GNWs) on Cu foil, nickel foam, and glass	• 50, 200, 300 mV/s were 0.053, F cm^{-3} at 50 mV/s • 0.049 F cm^{-3} at 200 mV/s 0.047 F cm^{-3} at 300 mV/s	–	• 25.1 m^2 g^{-1} for GNWs	• Plasma-enhanced CVD • Morphology: curled nanowall • Sheets, average length of 1 μm • < 10% degradation after 800 cycles	• Potential range −0.3 to 0.5 V • SR 50–300 mV/s	[85]

*Specific capacitance of CMG material

Electrolyte	Cyclic voltammogram average (mV/s)			Galvanostatic discharge (mA)	
	20	40		10	20
KOH	100	107		135	128
TEABF4/PC	82	80		94	91
TEABF4/AN	99	85		99	95

PEE were in association with respect to tensile axis, and the consequent energy dissipation by the chain rearrangement was hindered due to the dispersed TRG.

Graphene quantum dots (GQDs) have received substantial interest for various applications in photovoltaic and biomedical imaging. In comparison to graphene, the GQDs offered more edge sites which lead to enhanced absorption of the ionic charge [89]. In this paper, the authors had prepared activated GQD (aGQDs) using facile ultrasonic route with chemical activation using KOH as shown in Fig. 11. For the production of homogeneous aGQDs, FLGs (few layer graphene sheets) were employed as the starting material. The calculated specific capacitance of aGQDs film on GCE was 236 F g^{-1}, which was much higher in comparison to 172 F g^{-1} of aFLGs (activated few layer graphene sheets), 108 F g^{-1} for GQDs and 63 F g^{-1} for FLGs. Due to the slower ion diffusion and increased charge transfer resistance, the deviation in the capacitance was observed. This was the major drawback suffered by this synthesis route.

Rechargeable zinc battery has been a highly recommended option for energy conversion and storage. A zinc/graphite-based dual ion rechargeable battery had been fabricated using metallic zinc as anode and graphite material as cathode [90]. Since aqueous electrolytes suffer from the drawback of narrow potential window, hence, the authors have used ionic liquid-based electrolyte with electrochemical window of 2.8 V. The morphology obtained from the SEM images reveals the uniform distribution of dense and compact zinc deposits of average size 200 nm on anodes. The columbic efficiency of 93.5% for 100 cycles was delivered by the cell which possessed an energy density of 65.1 Wh/kg and 33.7mh/kg discharge capacity. Though the cell was cost effective but suffered from the drawback of low cycle stability [90].

Titanium oxide (TIO_2) with wide energy band gap (ranging from 3 to 3.25 eV) offers high binding energy, effective photo catalytic activity, and tunable crystal structure. Nanostructure TiO_2 has emerged out as effective photo catalytic which can effectively eliminate the environment pollutants. An efficient, low cost, and robust techniques to be developed for removing dyes from the waste water as the organic dyes constitute largest group of harmful environment pollutants which are discharged into rivers and streams from the industries. The hybrid photocatalysts with one or more functional attachment and active component were recommended. Doping the hybrid photocatalysts with metals and non-metals reported back in literature has improved the photocatalytic performance. Some reports have shown conducting polymer with ceramic and metal oxide nanomaterials providing outstanding electrochemical properties. For maximizing the photo catalytic activity, a variety of TiO_2 polymer-based nano/microstructures like 0D particles/spheres, 1D nanowire fibers, 2D nanosheets, and 3D hierarchical structures had been synthesized in the recent years [91]. Apart from organic pollutants' decomposition,

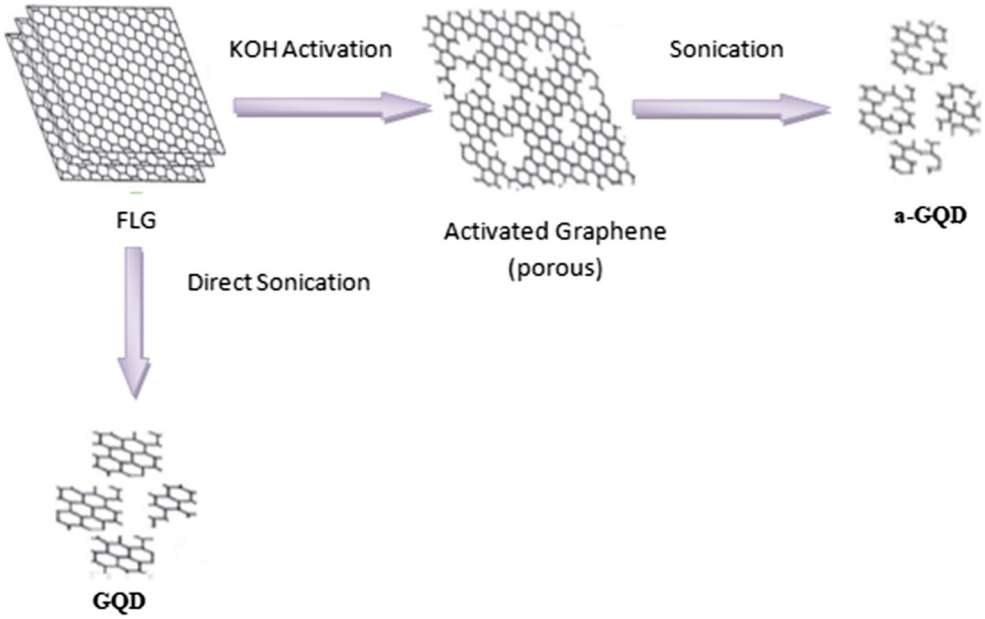

Fig. 11 Steps for preparing GQDs and aGQDs from FLGs [89]

other applications like hybrid solar cells, photo detectors, gas contaminants, and water splitting needs to be understood and applied.

As per a latest report, nanostructured PANI in various other different morphologies was composited with the graphene sheets to yield potential electrode material for supercapacitor. Hydrothermal assistant chemical oxidation polymerization synthesis route was used for composting PANI layers with GNS (graphene nanosheets) whereas for the synthesis of PANI nanofibers (diameter in range 50–100 nm), one step hydrothermal synthesis method was employed. The observed GNS/PANI composites delivered specific capacitance in the range of 532–304.9 F/g at scan rate in the range of 250 mV/s. The obtained retention rate was ~99.6% which ensures its great potential as an electrode material for supercapacitor.

Activated carbons (ACs)

Activated carbon is the most importantly the demanding material for the fabrication of the supercapacitor electrodes. The high surface area and the low cost make them the widely preferred active material for electrodes. These materials are obtained from carbon-rich organic precursors which can be easily derived from natural renewable sources like wood, coconut shells, fossil fuels, or from their derivates like pitch coal. AC is also obtained from synthetic precursors like polymers [92]. Table 3 gives the summary of precursors along with the corresponding BET surface area values for AC derived from these precursors.

The carbonization process helps in the production of amorphous carbon and the thermal chemical conversion of the precursors, and the activation process leads to the high surface area. This is achieved using partial controlled oxidation of carbon precursor grains either by physical or chemical activation. The chemical activation is carried on the amorphous carbons which were previously mixed with chemicals (e.g., carbonates, chlorides, alkalis) or acids (like K_2CO_3, KOH), whereas the physical activation is performed under oxidizing atmosphere (like H2O, Co_2) at high temperature. Any of the activation methods used, there is a bulk formation of porous network possessing high specific surface area carbon particles.

Table 3 Carbon precursors with their BET specific surface area. Data taken from [93]

Carbon precursor	S_{BET}	Activation method
Apricot shell	2335	NaOH
Banana fiber	1100	$ZnCl_2$
Bamboo	1290	KOH
Beer lees	3560	KOH
Cellulose	2460	KOH
Coconut shell	1660	KOH
Corn grain	3200	KOH
Coffee ground	1020	$ZnCl_2$
Eucalyptus wood	2970	KOH
Fish scale	2270	–
Firwood	1130	Steam
Potato starch	2340	KOH
Rice husk	1890	NaOH
Starch	1510	KOH
Sucrose	2100	CO_2
Sugarcane bagasse	1790	$ZnCl_2$
Wheat straw	2316	KOH

S_{BET} BET surface area

The theoretical specific surface area of ACs is 3000 $m^2\ g^{-1}$, though the reported usable surface area in literature is in the range of 1000 to 2000$m^2\ g^{-1}$. Most of the commercially available devices employing AC as electrode materials operate at cell voltages of 2.7 V. The specific capacitance of 100 to 120 F g^{-1} [94, 95] and volumetric capacitance up to 60 F cm^{-3} were reported [96]. The electrodes employing aqueous electrolyte had limited cell operating voltage of up to 0.9 V [92] and the specific capacitance of value 300 F g^{-1} [97].

A work in the past focused on using three types of ACs monolithic as electrode in half-cell electrochemical systems. Because of grain formation during oxidation, the porosity and surface area were improved. Maximum capacitance values obtained were 27.68 F g^{-1}, 2.23 F g^{-1}, and 1.20 F g^{-1} for the acid, steam oxidized, and non-oxidized electrodes respectively [98].

As per the report, the energy density of 1.27Whkg^{-1} and the specific capacitance of 100 F g^{-1} were obtained for graphene-gold nanoparticle composite [99]. In a paper, highly porous graphene-based carbon was fabricated. The obtained carbons gave rise to Brunauer-Emmett-Teller (BET) surface area of value up to 3290 $m^2\ g^{-1}$. The obtained specific capacitances were 174 F g^{-1} (gravimetric) and ~ 100 F cm^{-3} (volumetric). Gravimetric energy and power density values observed were 74 Wh kg^{-1} and 338 kW kg^{-1} respectively and volumetric values were 44 Wh L^{-1} and 199 kW L^{-1} respectively [75]. As per a report, BET surface areas of 1552 $m^2\ g^{-1}$ for apple-peel-based AC and 1103 $m^2\ g^{-1}$ for apple-pulp-based AC were reported [100].

Recently, the ACs were obtained by the carbonization of waste of fiberboards (medium density) at 500 °C. The activation was carried using KOH electrolyte at 800 °C with varying KOH/coke mass ratio. The surface area in the range of 1456 to 1647$m^2\ g^{-1}$ was obtained for both types of pores (micropores and mesopores). The specific capacitance ranging from 212 to 223 F g^{-1} was obtained for AC electrodes [101].

Carbon nanotubes (CNTs) and carbon nanofibres (CNFs)

Different carbon nanomaterials such as carbon nanofibres (CNFs), graphene nanofoam, carbon nanotubes (CNTs), graphene, and reduced graphene oxide (rGO) possess good intrinsic physical properties like electrical, chemical, mechanical, and thermal. Apart from these, they have unique morphological properties which are size and surface dependent and also ideal for their use and application in semiconductors.

Since their discovery, CNTs and CNFs have gathered special attention in being a strong member of novel electrochemical materials [102].

CNTs and CNFs are developed by the chemical decomposition of various hydrocarbons. Different nanostructured formations can be obtained by manipulating the different parameters; SWCNTs and MWCNTs can be formed. Both of these possess high electrical conductivity and good accessible surface area. The purity and morphology of the material influence the specific capacitance of CNTs. They can also be developed without the help of any binder in a conductive substrate. This process reduces the resistance value between current collector and the active material, which in turn simplifies the electrode fabrication. Many research efforts in the literature suggest the development of dense and aligned CNT forest which could help to increase capacitance retention at high current by adjusting and tuning the distance between the tubes. Single-wall CNTs are formed by rolling graphene sheets into nanoscale tube form. Furthermore, additional graphene tubes may be present around the core of single-wall CNT (SWNT) to yield multi-wall CNT (MWCNT) which includes the double-wall CNT (DWNT).

Different synthesis routes for CNTs have been suggested such as carbon arc-discharge [103, 104], pulsed laser vaporization [105, 106], SWNTs pyrolysis of hydrocarbons [107], CVD for aligned MWCNT [101, 108], and for aligned SWNTs, the plasma enhanced CVD method [109].

CNTs have turned out to be the attractive material for electrodes because of its some novel properties like high specific surface area, very high mesoporosity, good electrical conductivity, high electrolytic accessibility, and high capability of charge transport [110, 111]. Vertically aligned CNTs have turned out to be more advantageous over their counterparts that were randomly entangled [112]. A large number of reports have been suggested in literature demonstrating the rate capability improvement of aligned CNTs over the randomly entangled CNTs [113–119]. A high specific capacitance of 440 F g^{-1} was observed for the aligned CNT using template-free CVD mechanism in ionic liquid electrolyte [120–122]. A high energy and power density of 148 Wh kg^{-1} and 315 kW kg^{-1} was also observed. The CNTs coated with titanium nitride in 0.5 M H_2SO_4 electrolyte showed a specific capacitance of 81 m F cm^{-2} [123].

Due to the hydrophobic property of CNT, a low specific capacitance in the range of 20–80 F g^{-1} was obtained for purified CNTs powders. By using the subsequent oxidative processes, the specific capacitance up to 130 F g^{-1} was achieved. The oxidative treatments used modified the surface texture and also introduced additional surface functionality which contributed to the pseudo capacitance. The catalytically grown MWCNT with 8 nm diameter and BET surface area of value 250 $m^2\ g^{-1}$ was reported earlier. They were further treated with nitric acid to form electrodes which consisted of free standing mats of entangled CNTs having a large surface area of value 430 $m^2\ g^{-1}$, though this mat had negligible microporosity with average pore diameter of 9.2 nm. The interstitial spaces which were created by the entangled network of nanotubes contributed much of the CNTs porosity. On treatment with sulfuric acid, specific capacitance of 102 F g^{-1} at 1 Hz with power density of more than 8 kWkg^{-1} was observed.

Later on, the chemical activation of CNT with KOH for increased surface area while maintaining the nanotubes morphology was suggested by few authors [124]. These treatments helped to achieve an increased BET surface area from 430 to 1035m^2 g^{-1}. The value of specific capacitance in alkaline media was reported to be 90 F g^{-1} (8.7 μF cm^{-2}) and in non-aqueous media it was reported as 65 F g^{-1} (6.2 μF cm^{-2}).

Authors have grown some well-aligned MWCNTs on aluminum film of length 1–10 μm and diameter in the range of 5–100 nm which achieved very high power density and 120 F cm^{-3} volumetric specific capacitance [125, 126]. The CNTs with limited specific surface area and moderate capacitance value had suggested the creation of composites using both CNTs and conducting polymers (CPs). These composites offer the advantage of electric double-layer capacitance and pseudo capacitance of CNTs and CNFs respectively which helped in achieving higher capacitance. In situ chemical polymerization route was used for the preparation of composites which led to the formation of uniform coating on CNT surface.

A high specific capacitance of value 170 F g^{-1} was achieved by electrodepositing MWCNTs with polypyrrole. Degradation of the polymer made it hard to achieve a cycle life greater than 1 lakh cycles. Similar composites using SWCNTs achieved higher specific capacitance up to 265 F g^{-1}. The PPy acted as a conducting agent in these composites which helped in reducing the ESR (equivalent series resistance) of the supercapacitor. The overcharging and overdischarging of the supercapacitor during operation had accelerated the degradation of these composites. Hence, carbon-supported transition metal oxides have emerged as an alternative. Higher specific capacitance of 80 F g^{-1} was reported by the introduction of 1 wt% of RuO_2 into MWCNT electrode. Apart from this, longer cycle life in comparison to CNTs coated with conducting polymers was also observed.

The hydrophobic nature of MWCNTs and the longer reaction time consume by the nanoparticles for their generation restricted the dispersion of various metal nanoparticles into CNTs. The hydrophobic nature of MWCNTs did not allow the metal nanoparticle to be held to their surface. Also, the longer reaction time consumed by the nanoparticles for their generation restricted the dispersion of various metal nanoparticles into CNTs. To combat these short comings, ϒ irradiation synthesis method was proposed for the formation of nanoparticles which minimized the nanoparticle generation reaction time [127]. For effective dispersion of nanoparticles, CNT functionalization with further more adaptable/soluble PANI derivates like SPAN (sulfonated polyanniline) was suggested. The observed conductivity of value 1.55 Scm^{-1} for MWCNT-SPAN-M composite was very much higher than SPAN which had conductivity of 2.46 Scm^{-1}. Table 4 gives an overview of different performance parameters of CNTs-based electrode materials.

Table 4 Overview of performance parameters of CNTs based electrode materials

Electrode material type	Electrolyte used	Growth process	Specific capacitance (F/g)	Specific surface area (m^2/g)	Energy density (Wh/kg)/ power density (kW/kg)	Ref no.
CNTs	$TEABF_4$/AN (4 V)	Vapour-phase catalyst delivery CVD	61.2	–	8.5/~ 7 at scan rate 1000 mV/s	134
MWCNTs	6 MKOH (1 V)	CVD	18 and 61.2 with 0.022 mol l^{-1} complex mixture concentration	365 –for Fe:Co (2:3) after 30 min 248 for same catalyst on Ni foil after 20 min	7	135
AMWCNTs	(Et_4) NBF_4/PC (2.5 V)	CVD	83 at 1 mV s^{-1} 47 at 1000 mV s^{-1}	150 μm in length	0.53 Ω ESR	136
SWCNTs	Al coating of AL_2O_3	WACVD (750 °C)	140	6	0.05 and 0.5/-	137
CNTs. no binder	$1MH_2SO_4$ (1 V)	Suspension	39	–	0.02/5.8	138
Carbon cloth/CNTs	0.5 MNa_2SO_4 (2 V)	MPECVD	225	724.8	28 Wh/kg 87% after 10 k cycles	139
VASWCNTs	1 M $TEABF_4$/PC	WACVD	66	561	27/987	140
CNTs Purification and activation + binder	6 M KOH, 1 M H_2SO_4, 1.4 M TEABF4 AN (2 V)	TCVD	15 to 90 - in alkaline medium (6 M KOH) 65- in organic electrolyte	1050	–	142

SWCNT films used with chlorosulfonic acid obtained at 120 Hz were also investigated for ac line filtering which showed specific capacitance of 601 μF cm^{-2} [128]. On further investigation, SWCNTs showed a specific capacitance of 282 μF cm^{-2} at 120 Hz when used with the organic electrolyte. This result showed that the value of capacitance for film thickness range 53–298 nm was increasing but was decreasing on further increasing the thickness [110]. A volumetric capacitance at 20 Hz and at 100–20 kHz was obtained as 23 mF cm^{-3} and 6 mF cm^{-3} for CNTs which were coated with Al_2O_3 dielectric [129]. Different treatments have also been tried in the literature for improving the electrical conductivity and the surface area of the CNTs [127, 128]. Such treatments include the doping, functionalization, activation, and the opening of walls from the top and side. The specific capacitance of 11 F g^{-1} and energy density of 24.7 Wh kg^{-1} was achieved for SWCNTs by opening the top and side walls [132]. Solid state supercapacitors were also designed to be used at high frequencies. Supercapacitors designed with coating of MWCNTs with Al_2O_3 dielectric achieved a specific capacitance of 25 mF mm^{-2} for frequency up to 1 MHz [133].

The specific capacitance in the range of 40–300F/g [19, 134] had been reported in the literature for the EDLC supercapacitors. In contrast to this, the next-generation energy storage promising candidate carbon nanomaterial metal-oxide supercapacitors (CNMO-SC) have shown ultra high specific capacitance (> 100 F/g) with good energy density and maintaining cost effectiveness. Hence, we present a review of certain types of CNMs.

As per a report, nanostructured brush using CNT composites in colloidal system with PS (polystyrene) has been synthesized using in situ polymerization route [135]. FTIR analysis confirmed the effectiveness and the bond formation of the PS/CNT composites. The BET surface area for PS/CNT (10%wt) was 431.9m^2/g and the corresponding pore volume was observed as 1.48cm^3/g. As per the analysis, the increase in wt% not only increased the pore volume but also improved its BET surface area. Increased SSA (specific surface area) and the pore volume are correlated with the composites-enhanced gas adsorption properties. Hence, CNT with high BET surface area in polymer composite has emerged as a promising candidate for future supercapacitors.

The development of conducting 1D PTh (polythiopene) nanofibers in hollow TiO_2 nano tube arrays by controlled nucleation and growth during electro polymerization of thiophene monomer was demonstrated in one of the papers [136]. For achieving the advantage of detailed kinetic study of thiophene polymerization by on-line monitoring of characteristics of growth during polymerization, the process of electrochemical polymerization of thiophene was carried out by cyclic potential sweeps in window of (− 0.6 to 2 V). These FE-SEM images of TNTs and PTh-NFs showed that the number of NFs increased on increasing the concentration of the monomer. But further increment of the concentration to 1.0 M distorted the NFs which resulted due to the overgrowth or polymer swelling. The observations further showed that the scan rates played an important role in the formation of PTh-NFs. On selecting 0.5 M thiophene concentration at scan rate of 5 mVs^{-1}, the tips of NFs appeared at the open ends of TNT, while a different morphology of continuous and abundant growth was observed at 15 mV s^{-1} scan rate. The appearance of relatively more vertical lines which is an indication of obstruction to ion diffusion in Nyquist plot supported the justification of the excellent charge storage (observed specific capacitance 1052 F g^{-1}) mechanism in the PTh-TNT NFs as compared to 45° sloped lines of other morphologies of PTh. According to the following equation, reduced ion diffusion length was observed in 1D PTh-TNT NF. The formed 1D polymer NS possessed good molecular conformation, high doping levels (for excellent redox properties), and excellent conductivity as high as 142 Scm^{-2}:

$$t = \frac{l^2}{D} \tag{6}$$

where

t ion diffusion time through supercapacitor electrode
l diffusion length
D diffusion constant

Carbon nanomaterials-metal oxide-based supercapacitor (SC)

Graphene/reduced graphene oxide (rGO) metal-oxide-based SC

Graphene is a well-known material possessing specific surface area of value 2620 m^2/g (theoretically). Different strategies have been adopted in the past using graphene coupled with MnO_2 [137], MoO_3 [138], Mn_3O_4 [139], Co_3O_4 [140], and $CoMoO_4$ [141]. Planar SC was fabricated by using δ-MnO facial assembly and flakes of reduced graphene oxide (rGO) [142]. The interactions induced due to morphologically and the synergic effects because of electrostatic effects have enhanced the rGO and MnO_2 nanosheets integration. Synthesis of graphene aerogels (GA) has also been reported in the same year using sol-gel method [143]. The synthesized GA possessed good specific surface area (793 m^2/g), high pore volume (3 cm^2/g), and good specific capacitance of value 410 F/g. The 3D network of GA support and the structural advantages have resulted in good stability (decaying 5% in 50,000 cycles) and capacity (410 F/g). An outstanding mechanical and electrical property of 3D graphene foam was demonstrated in the past. This was done by the CVD synthesis of graphene foam (GF) on nickel foam (NF). This was further

followed by the Mno_2 [137] and $CoMoO_4$ [141] hydrothermal deposition. Since graphene has good conductance and mechanical support, it does not require any other metal current collector. The specific capacitance of 144 F/g and 439.7 F/g for GF-Ni (OH) and GF-$CoMoO_4$ was obtained respectively. They had power density of 44 W/kg and 900 W/kg respectively which depict its usage for flexible and stretchable SCs due to its superior electrochemical and structural property.

A group of researchers have also reported about the graphene nanocomposites using an in-solution process [138, 140] with the Co_3O_4 and Mn_3O_4. Mentioning specifically, synthesis of graphene oxide (GO) was first done with Hummer's method. Later on, the precursor solution were intermixed with the graphene oxide. Further for depositing Mn_3O_4/Co_3O_4 onto the rGO thermal and microwave, assist treatment was carried out. The cobalt oxide nanoparticle microwave-assisted intercalation was also proposed using graphene wrapping [144].

Nanostructured carbon-based electrode material are most widely used for the electrochemical applications because of its low cost, good electrical property, thermal and chemical stability, and good reversible redox reaction feasibility. However, these do not offer good energy density-high specific capacitance and stable cycle life. Hence, for overcoming these defects, they are mostly coupled with the metal oxides. Thus, the designing of an electrode with flexible CFF (carbon fiber foam) and MnO_2 had been an edge cutting research that contributed to the electrochemical behavior during both charging and discharging period. CFF was chosen for the current collector due to its high corrosion resistance, low cost, easy fabrication, 1D structure, and high electrical conductivity. MnO_2 had been recognized as a promising candidate for its simple synthesis process.

Few researchers have developed a solid state highly flexible CFF/MnO_2-based electrode material for supercapacitor applications. Hydrothermal method was used to functionalize CFF with coral-like MnO_2 nanostructure for the improvement of the pseudo capacitive properties [145]. The specific capacitance of 467 F g^{-1} with 100% initial capacitance maintenance after 5000 cycles was attributed to the presence of unique structure of the electrode which enabled fast ion diffusion. Apart from these, an energy density of 20 Wh/kg and faster charge and discharge rates were observed. Morphology of the thermally aged CFF and CFF/MnO_2 hybrids was analyzed after reaction at 175 °C. The observations made the FE-SEM images revealed that the interaction between CFF and MnO_2 was quite strong and the CFF acted as a good substrate. In addition to these, an energy density of 20 Wh/kg and power density of 0.175 kWh/kg was demonstrated for the devices fabricated with CFF/MnO_2.

Carbon fiber paper-metal oxide-based supercapacitors

Carbon nanofiber paper exhibits good mechanical and electrical properties along with easy scaling. It is well-known as carbon cloth or carbon fabric as it contains large amounts of micro-sized fibers whose diameter is in the range of 5–15 μm. In the literature, $NiCo_2O_4$ has emerged to be the most frequently used metal oxide material with carbon fiber paper (CFP) in various forms. It is also coupled as CFP-$NiCo_2O_4$@NiO [146], CFP-Ni/Co-layered double hydroxide (LDH)@ZnO [147–149] and precursor ($NiCo_2O_4$) [148] was electrodeposited to get ultra thin nanosheets arrays. The good conductivity of composites along with the interconnected structure has resulted in good specific capacitance of value 2658 F/g and cyclic stability.

Apart from $NiCo_2O_4$, different other composites like $NiCo_2S_4$ and VO_x have also been integrated which served as an excellent pseudocapacitive material [150, 151]. $NiCo_2O_4$ single crystal grown on CFP has facilitated the ion diffusion process. Various methods of diffusion have been reported in the past for depositing NiO and VO_x like hydrothermal, elctrodeposition, and dip coating [152, 153]. These composites have resulted in good and better performance energy storage devices, and overview of few composites has been given in Table 5.

Electrospun CNF metal oxide-based SCs

CNF and CFP are nearly the same material possessing tens of micrometers of length and diameter in the range of 30–220 nm. Just like CFP, ECNF has good electrical conductivity, large porosity, and high mechanical stability. Due to its reliable 3D structure, it can support the nanostructured metal oxide

Table 5 Overview of composites

Material fabricated	Method followed	Comments	Ref. No.
$NiCo_2O_4$ @ NiO-CFP (hetero-nanowire)	Step-wise dip coating	Specific capacitance (1500–1900)F/g	161–162
Ni/Co LDH	Electrodepositing $CoNi_{1-x}$ hydroxide coatings on CFP supported nanowire arrays	Energy density (33–45)Wh/kg	163
CFP-Ni/Co LDH @ ZnO	Two-step hydrothermal analysis	Power density (41–46)kW/kg	164

uniformly [154]. A deep investigation on ECNF has been carried out in the past using various synthesis methods like dip coating, electrochemical deposition, and activation treatment [154, 155]. Activated ECNF was coupled using SnO_2 [156], Co_3O_4 [157], V_2O_5 [158], and ZnO [159]. This was achieved by the incorporation of different metal oxide precursors like V_2O_5 in DHF, $SnCl_2.2H_2O$, Ca $(acac)_2$ and $Zn(O_2CCH_3)_2$.

The method of one-step electro spinning was used for the coupling of ECNF. The cyclic stability reported in these electrodes was very low due to the internal structure of ECNF network. Although the specific surface area showed an increased value of (> 1000 m^2/g) as compared to (< 100 m^2/g) for the non-activated ECNF [160]. Figure 12 shows setup for the preparation process of the hollow Co_3O_4 NPs-CNFs. Dip coating offers a simple yet cost effective technique for depositing metal oxide onto the ECNF. This method has been employed for a wide range of voltage value varying from 0–2 V. Electro deposition offers quantitative control of morphology of metal oxide materials.

Hybrid carbon nanomaterials–metal oxide-based supercapacitors

Various carbon materials like graphene, carbon nanosheets, carbon nanofibres, and carbon nanotubes have served to be the important materials for huge energy storage applications. Each of the materials has their own significant properties in terms of physical, electrical, and morphological. Hence, structures comprising of different carbon nanomaterials have emerged to be the material of interest as they have their own intrinsic properties and also exhibit new characteristics offered by new elements.

Graphene foam was used with the CNT for high performance SCs. Literature shows the use of graphene foam with MnO_2, RuO_2, and Fe_2O_3 using ALD (atomic layer deposition) and modified sol-gel method for obtaining CNT forest hybrid structures [153, 161]. Novel graphite foam CNT forest decorated with iron oxide has been developed by Guan et al. [161] giving specific capacitance of large value as 2555.6 F/g. The graphene@CNT on nickel foam and dip coating for depositing MnO_2 and RuO_2 on to the hybrid structures have resulted in superior designs that provided large surface area for metal deposition, conductive 3D network, and cost effective synthesis [162]. New approaches have been suggested by employing graphene nanosheets coupled with CNT/CNF. The deposition of MnO_2 [163], Ni $(OH)_2$ [164], and Fe_2N [165] onto graphene flakes has been reported in the past using various deposition processes like ALD, thermal-assisted chemical coating, and hydrolysis/condensation. Table 6 reports collective results of different carbon nanomaterial–metal oxide-based semiconductor for various energy storage applications.

Conclusion and future scope

Electrode materials based on graphene with different architecture exhibit good mechanical, chemical, and physical behavior. This helps in improving the electrochemical performance of the energy storage devices. The addition of mesopores in small amount onto micropore surface increases the power capability of the ultracapacitors. From the available representative results and comparisons, we can draw certain conclusions and future scope of work:

- Carbon nanomaterials have excellent conductivity, large surface area, good mechanical properties, cost effective, and feasibility towards chemical modifications which make carbon nanomaterial as a promising candidate for energy storage systems.
- The metal oxide with 3D support like graphene foam, reduced graphene oxide, carbon nanofiber, carbon nanopaper, and electrospun CNF have also been preferred for high-performance supercapacitors. Despite being a

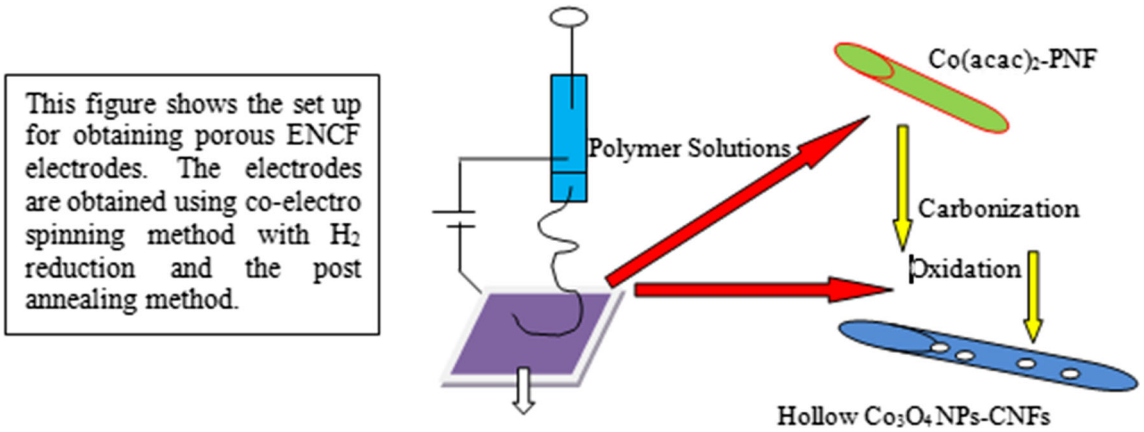

Fig. 12 Setup for the preparation process of the hollow Co_3O_4 NPs-CNFs

Table 6 Summary of different carbon nanomaterial–metal oxide-based semiconductor

Electrode materials	Metal oxide materials		Specific capacitance (F/g)	Energy density (Wh/kg) power density (kW/kg)	Stability	Ref. No.
	Method	Materials				
A. Graphene/reduced graphene oxide (rGO)–metal oxide-based SC						
Graphene foam (GF)	Hydrothermal	MnO_2	240	8.3/20	90% 1000 cycles	[137]
Graphene foam (GF)	Hydrothermal	$CoMoO_4$	2741	37.25/0.9	87.4% 10,000 cycles	[141]
Reduced graphene (rGO)	Layer-by-layer deposition	Mn_3O_4	344	93/10	87% 3000 cycles	[139]
Reduced graphene (rGO)	Microwave coating	MoO_2	404	55/0.4	80% 5000 cycles	[138]
B. Carbon nanofiber/carbon fiberpaper/electrospun CNF (ECNF)						
CNF	Chemical growth	MnO_2	56.8	30.6/0.20	94% 5000 cycles	[166]
CFP	Thermal-chemical growth	$NiCo_2O_4$	942	–/–	96.4% 2400 cycles	[150]
CFP	Hydrothermal	VO_x	298	0.61 mWh/cm^3/0.85 W/cm^3	87.5% 10,000 cycles	[151–153]
ECNF	Co-electro-spinning	SnO_2	289	7.7/8	97% 3000 cycles	[156]
ECNF	Co-electro-spinning	V_2O_5	74	68.5/20	- -	[158]
C. Carbon nanomaterial hybrid based						
GF + CNF	ALD	Fe_2O_3	2555	74.7/1.4	95.4% 50,000 cycles	[153]
GF + CNF	Sol-gel	RuO_2	503	39.3/128	106% 8100 cycles	[162]
rGO + CNT	Thermal growth	MnO_2	126	28.33/5	83% 2500	[161]
CNF + G	ALD	FeN	58	15.4/6.4	99% 20,000 cycles	[165]
CNF + rGO	EC-deposit	Ni $(OH)_2$	1235	–/–	80% 500 cycles	[164]
CFP + rGO	Chemical	MnO_2	393	–/–	98.5 2000 cycles	[163]

good candidate, it has the drawback of having low power density in comparison with lithium-ion battery.

- From the literature, it can be deduced that tunable 3D graphene network consisting of interconnected porous structure is more preferred over 0D, 1D, and 2D as its structure can be manipulated for obtaining good ion/charge pathways and large interstitial surface area.
- Hybrid carbon nanometal oxide-based materials have emerged as the new direction for the supercapacitor electrodes for addressing the synergetic effect, enhancing the charge storage and improving the overall cyclic performance of the device.
- Ultra high energy density and long cycle stability were achieved using hierarchical assembly of graphite foam-CNT coated with Fe_2O_3 (GF-CNT@Fe_2O_3). But this was achieved on the compromise of columbic efficiency (i.e., capacitance retention) and power density. On the contrary, high power density and efficiency were obtained for GNS@CF substrate on compromising the cycle stability.

Despite of various parameter advantages, there are certain challenges like cycle stability and energy density of the storage devices which are yet to be addressed.

References

1. Convay BE (1999) Electrochemical supercapacitors, scientific fundamentals and technological applications. Plenum, New York. https://doi.org/10.1007/978-1-4757-3058-6
2. Burke A (2000) J Power Sources 91:37. https://doi.org/10.1016/S0378-7753(00)00485-7
3. Zhang LL, Zhao XS (2000) Carbon-based materials as supercapacitor electrodes. Chem Soc Rev 38:2520. https://doi.org/10.1039/b813846j
4. Dulyaseree P, Yordsri V, Wongwiriyapan W (2016) Effects of microwave and oxygen plasma treatments on capacitive characteristics of supercapacitor based on multiwalled carbon nanotubes. Jpn J Appl Phys 55(2):02BD05. https://doi.org/10.7567/JJAP.55.02BD05
5. Frackowiak E, Delpeux S, Jurewicz K, Szostak K, Cazorla-Amoros D, B'eguin F (2002) Enhanced capacitance of carbon nanotubes through chemical activation. Chem Phys Lett 361(1–2):35–41. https://doi.org/10.1016/S0009-2614(02)00684-X
6. Ambade RB, Ambade SB, Shrestha NK, Salunkhe RR, Lee W, Bagde SS, Kim JH, Stadler FJ, Yamauchi Y, Lee S-H (2017) Controlled growth of polythiophene nanofibers in TiO2 nanotube arrays for supercapacitor applications. J Mater Chem A 5:172. https://doi.org/10.1039/c6ta08038c
7. Hassan M, Reddy KR, Haque E, Faisal SN, Ghasemi S (2014) Hierarchical assembly of graphene/polyaniline nanostructures to synthesize free-standing supercapacitor electrode. Compos Sci Technol 98:1–8. https://doi.org/10.1016/j.compscitech.2014.04.007
8. Reddy KR, Sin BC, Yoo CH, Park W, Ryu KS, Lee J-S, Sohn D, Lee Y (2008) A new one-step synthesis method for coating multi-walled carbon nanotubes with cuprous oxide nanoparticles. Scr Mater 58:1010–1013. https://doi.org/10.1016/j.scriptamat.2008.01.047
9. Xiao X, Wang G, Zhang M, Wang Z, Zhao R, Wang Y (2018) Electrochemical performance of mesoporous $ZnCo_2O_4$ nanosheets as an electrode material for supercapacitor. Ionics 24:2435. https://doi.org/10.1007/s11581-017-2354-9
10. Winter M, Brodd RJ (2004) What are batteries, fuel cells and supercapacitors? Chem Rev 104:4245–4269. https://doi.org/10.1021/cr020730k
11. Bard AJ, Faulkner LR (2013) Electrochemical methods - fundamentals and applications, 2nd edn. John Wiley & Sons, New York ISBN: 978—471-0437-0
12. Reddya KR, Sina BC, Ryua KS, Nohb J, Leea Y (2009) In situ self-organization of carbon black–polyaniline composites from nanospheres to nanorods: synthesis, morphology, structure and electrical conductivity. Synth Met 159(2009):1934–1939. https://doi.org/10.1016/j.synthmet.2009.06.018
13. Zhang LL, Zhao XS (2009) Carbon-based materials as supercapacitor electrodes. Chem Soc Rev 38:2520–2531. https://doi.org/10.1039/b813846j
14. Zhang H, Lv X, Li Y, Wang Y, Li J (2009) P25-Graphene composite as a high performance photo catalyst. ACS Nano 4:380–386. https://doi.org/10.1021/nn901221k
15. Gouy G (1910) J Phys Chem B 4:457
16. Chapman DL (1913) Philos Mag 6:475
17. Endo M, Takeda T, Kim Y, Koshiba K, Ishii K (2001) High power electric double layer capacitor (EDLC's); from operating principle to pore size control in advanced activatedcarbons. CarbonScience 1(3):117–128 URL ⟨http://carbonlett.org/Upload/files/CARBONLETT/117–128.pdf⟩
18. Stern OZ (1924) Electrochemistry 30:508. https://doi.org/10.1039/b813846j
19. Sharma P, Bhatti T (2010) A review on electrochemical double-layer capacitors. Energy Convers Manag 51(12):2901–2912. https://doi.org/10.1016/j.enconman.2010.06.031
20. Barbieri O, Hahn M, Herzog A, Kötz R (2005) Capacitance limits of high surface area activated carbons for double layer capacitors. Carbon 43(6):1303–1310. https://doi.org/10.1016/j.carbon.2005.01.001
21. Qu D, Shi H (1998) Studies of activated carbons used in double-layer capacitors. J Power Sources 74(1):99–107. https://doi.org/10.1016/S0378-7753(98)00038-X
22. Gamby J, Taberna P, Simon P, Fauvarque J, Chesneau M (2001) Studies and characterisations of various activated carbons used for carbon/carbon supercapacitors. J Power Sources 101(1):109–116. https://doi.org/10.1016/S0378-7753(01)00707-8
23. Shi H (1996) Activated carbons and double layer capacitance. Electrochim Acta 41(10):1633–1639. https://doi.org/10.1016/0013-4686(95)00416-5
24. Qu D (2002) Studies of the activated carbons used in double-layer supercapacitors. J Power Sources 109(2):403–411. https://doi.org/10.1016/S0378-7753(02)00108-8
25. Kim Y, Horie Y, Ozaki S, Matsuzawa Y, Suezaki H, Kim C et al (2004) Correlation between the pore and solvated ion size on capacitance uptake of PVDC-based carbons. Carbon 42(8–9):1491–1500. https://doi.org/10.1016/j.carbon.2004.01.049
26. Huang J, Sumpter BG, Meunier V (2008a) Theoretical model for nanoporous carbon supercapacitors. Angew Chem Int Ed 47:520–524. https://doi.org/10.1002/ange.200703864
27. Huang J, Sumpter BG, Meunier V (2008b) A universal model for nanoporous carbon supercapacitors applicable to diverse pore regimes, carbon materials, and electrolytes. Chem Eur J 14:6614–6626

28. Huang J, Sumpter B, Meunier V (2008) Theoretical model for nanoporous carbon supercapacitors. Angew Chem 120(3):530–534. https://doi.org/10.1002/ange.200703864
29. Feng G, Qiao R, Huang J, Sumpter BG, Meunier V (2010) Ion distribution in electrified micropores and its role in the anomalous enhancement of capacitance. ACS Nano 4(4):2382–2390. https://doi.org/10.1021/nn100126w
30. Frackowiak E (2007) Carbon materials for supercapacitor application. Phys Chem Chem Phys 9:1774–1785
31. Chen T, Dai L (2013) Carbon nanomaterials for high performance supercapacitors. Mater Today 16(7/8):272–280. https://doi.org/10.1016/j.mattod.2013.07.002
32. Xia JL, Chen F, Li JH, Tao NJ (2009) Measurement of the quantum capacitance of graphene. Nat Nanotechnol 4:505–509. https://doi.org/10.1038/nnano.2009.177
33. Booth TJ, Blake P, Nair RR, Jiang D, Hill EW, Bangert U et al (2008) Macroscopic graphene membranes and their extraordinary stiffness. Nano Lett 8:2442–2446. https://doi.org/10.1021/nl801412y
34. Lee C, Wei XD, Kysar JW, Hone J (2008) Measurement of the elastic properties and intrinsic strength of monolayer graphene. Science 321:385–387. https://doi.org/10.1126/science.1157996
35. Wu Z-S, Zhou G, Yin L-C, Ren W, Li F, Cheng H-M (2012) Graphene/metal oxide composite electrode materials for energy storage. Nano Energy 1(1):107–131. https://doi.org/10.1016/j.nanoen.2011.11.001
36. Novoselov KS, Geim AK, Morozov SV, Jiang D, Zhang Y, Dubonos SV, al e (2004) Electric field effect tin atomically thin carbon films. Science 306(5696):666–669. https://doi.org/10.1126/science.1102896
37. Liang JJ, Huang Y, Zhang L, Wang Y, Ma YF, Guo TY, Chen Y (2009) Molecular level dispersion of graphene into poly (vinyl alcohol) and effective reinforcement of their nanocomposites. Adv Funct Mater 19:2297–2302. https://doi.org/10.1002/adfm.200801776
38. Huang X, Qi XY, Boey F, Zhang H (2012) Graphene-based composites. Chem Soc Rev 41:666–686. https://doi.org/10.1039/C1CS15078B
39. Kim KS, Zhao Y, Jang H, Lee SY, Kim JM, Kim KS et al (2009) Large-scale pattern growth of graphene films for stretchable transparent electrodes. Nature 457:706–710. https://doi.org/10.1038/nature07719
40. He QY, Wu SX, Gao S, Cao XH, Yin ZY, Li H et al (2010) Organic photovoltaic devices using highly flexible reduced graphene oxide films as transparent electrodes. ACS Nano 4:5263–5268. https://doi.org/10.1021/nn1015874
41. Schedin F, Geim AK, Morozov SV, Hill EW, Blake P, Katsnelson MI et al (2007) Detection of individual gas molecules adsorbed on graphene. Nat Mater 6:652–655. https://doi.org/10.1038/nmat1967
42. He QY, Sudibya HG, Yin ZY, Wu SX, Li H, Boey F et al (2010) Centimeterlong and large-scale micropatterns of reduced graphene oxide films: fabrication and sensing applications. ACS Nano 4:3201–3208. https://doi.org/10.1021/nn100780v
43. Liang JJ, Xu YF, Huang Y, Zhang L, Wang Y, Ma YF et al (2009) Infraredtriggered actuators from graphene-based nanocomposites. J Phys Chem C 113:9921–9927. https://doi.org/10.1021/jp901284d
44. Park S, An J, Suk JW, Ruoff RS (2010) Graphene-based actuators. Small 2010;6(2):210–212. URL ⟨http://pubs.acs.org/doi/abs/10.1021/nl802558y⟩
45. Xie XJ, Qu LT, Zhou C, Li Y, Zhu J, Bai H et al (2010) An asymmetrically surface-modified graphene film electrochemical actuator. ACS Nano 4:6050–6054. https://doi.org/10.1021/nn101563x
46. Liang JJ, Huang Y, Oh J, Kozlov M, Sui D, Fang SL et al (2011) Electromechanical actuators based on graphene and graphene/Fe3O4 hybrid paper. Adv Funct Mater 21:3778–3784. https://doi.org/10.1002/adfm.201101072
47. Becerril HA, Mao J, Liu Z, Stoltenberg RM, Bao Z, Chen Y (2008) Evaluation of solution-processed reduced graphene oxide films as transparent conductors. ACS Nano 2:463–470. https://doi.org/10.1021/nn700375n
48. Brownson DAC, Kampouris DK, Banks CE (2011) J Power Sources 196:4873. https://doi.org/10.1016/j.jpowsour.2011.02.022
49. Pumera M (2010) Graphene-based nanomaterials and their electrochemistry. Chem Soc Rev 39:4146–4157. https://doi.org/10.1039/C002690P
50. Hummers WS, Offeman RE (1958) Preparation of graphitic oxide. J Am Chem Soc 80:1339–1339. https://doi.org/10.1021/ja01539a017
51. Kovtyukhova NI, Ollivier PJ, Martin BR, Mallouk TE, Chizhik SA, Buzaneva EV, Gorchinskiy AD (2009) Layer-by-layer assembly of ultrathin composite films from micron-sized graphite oxide sheets and polycations. Chem Mater 11:771–778. https://doi.org/10.1021/cm981085u.
52. Park S, Ruoff RS Chemical methods for the production of graphenes. Nat Nanotechnol 4:217–224. https://doi.org/10.3390/lubricants2030137
53. Matsumoto H, Imaizumi S, Konosu Y, Ashizawa M, Minagawa M, Tanioka A, Lu W, Tour JM (2013) Electrospun composite nanofiber yarns containing oriented graphene nanoribbons. ACS Appl Mater Interfaces 5:6225–6231. https://doi.org/10.1021/am401161b
54. Zhang J, Wang K, Guo S, Wang S, Liang Z, Chen Z, Fu J, Xu Q (2014) One-step carbonization synthesis of hollow carbon nanococoons with multimodal pores and their enhanced electrochemical performance for supercapacitors. ACS Appl Mater Interfaces 6:2192–2198. https://doi.org/10.1021/am405375s
55. Vivekchand SRC, Rout CS, Subrahmanyam KS, Govindaraj A, 2008 R CNR Graphene-based electrochemical supercapacitors. J Chem Sci 120(1):9–13. https://doi.org/10.1007/s12039-008-0002
56. Stoller M, Park S, Zhu Y, An J, Ruoff R (2008) Graphene-based ultracapacitors. Nano Lett 2008;8(10):3498–3502. URL: ⟨http://pubs.acs.org/doi/abs/10.1021/nl802558y⟩.
57. Wang Y, Shi Z, Huang Y, Ma Y (2009) Supercapacitor devices based on graphene materials. J Phys Chem C 113(30):13103–13107. https://doi.org/10.1021/jp902214f
58. Yu K, Lu G, Bo Z, Mao S, Chen J (2011) Carbon nanotube with chemically bonded graphene leaves for electronic and optoelectronic applications. J Phys Chem Lett 2:1556–1562. https://doi.org/10.1021/jz200641c
59. Song Y, Xu J-L, Liu X-X (2014) Electrochemical anchoring of dual doping polypyrrole on graphene sheets partially exfoliated from graphite foil for high performance supercapacitor electrode. J Power Sources 249:48–58. https://doi.org/10.1016/j.jpowsour.2013.10.102
60. Cai Y, Wang Y, Deng S, Chen G, Li Q, Han B et al (2014) Graphene-tungsten oxides composite for supercapacitor electrode. Ceram Int 40(3):4109–4116. https://doi.org/10.1016/j.ceramint.2013.08.065
61. Deng L, Wang J, Zhu G, Kang L, Hao Z, Lei Z et al (2014) RuO_2/graphene hybrid material for high performance electrochemical capacitor. J Power Sources 248:407–415. https://doi.org/10.1016/j.jpowsour.2013.09.081
62. Wang D, Min Y, Yu Y, Peng B (2014) A general approach for fabrication of nitrogen doped graphene sheets and its application in supercapacitors. J Colloid Interface Sci 417:270–277. https://doi.org/10.1016/j.jcis.2013.11.021
63. Gopalakrishnan K, Govindaraj A, Rao CNR (2013) Extraordinary supercapacitor performance of heavily nitrogenated graphene

oxide obtained by microwave synthesis. J Mater Chem A 1(26): 7563. https://doi.org/10.1039/c3ta11385j
64. Choi BG, Yang M, Hong WH, Choi JW, Huh YS (2012) 3D macroporous graphene frameworks for supercapacitors with high energy and power densities. ACS Nano 6:4020–4028. https://doi.org/10.1021/nn3003345
65. Cheng Q, Tang J, Shinya N, Qin L-C (2013) Polyanniline modified graphene and carbon nanotube composite electrode for asymmetric supercapacitors of high energy density. J Power Sources 241:423–428. https://doi.org/10.1016/j.jpowsour.2013.04.105
66. Wanga Z, Maa C, Wanga H, Liu Z, Hao Z (2013) Facilely synthesized Fe2O3–graphene nanocomposite as novel electrode materials for supercapacitors with high performance. J Alloys Compd 552:486–491
67. Xie Q, Zhou S, Zheng A, Xie C, Yin C, Wu S, Zhang Y, Zhao P (2016) Sandwich-like nitrogen-enriched porous carbon/graphene composites as electrodes for aqueous symmetric supercapacitors with high energy density. Electrochim Acta 189:22–31. https://doi.org/10.1016/j.electacta.2015.12.087
68. Yang M, Lee KG, Lee SJ, Lee SB, Han Y-K, Choi BG (2015) Three-dimensional expanded grapheneemetal oxide film via solid-state microwave irradiation for aqueous asymmetric supercapacitors. ACS Appl Mater Interfaces 7:22364–22371. https://doi.org/10.1021/acsami.5b06187
69. Stoller MD, Park S, Yanwu Z, An J, Ruoff RS (2008) Graphene-based ultracapacitors. Nano Lett 8(10):3498–3502 URL: ⟨http://pubs.acs.org/doi/abs/10.1021/nl802558y⟩
70. Vivekchand SRC, Rout CS, Subrahmanyam KS, Govindaraj A, Rao CNR (2008) Graphene-based electrochemical supercapacitors. J Chem Sci 120(1):9–13. https://doi.org/10.1007/s12039-008-0002-7
71. Wu Z-S, Wang D-W, Ren W, Zhao J, Zhou G, Li F, Cheng H-M (2010) Adv Funct Mater 20:3595. https://doi.org/10.1021/nn900297m
72. Yang X, Zhu J, Qiu L, Li D (2011) Bioinspired effective prevention of restacking in multilayered graphene films: towards the next generation of high-performance supercapacitors. Adv Mater 23(25):2833–2838. https://doi.org/10.1002/adma.201100261
73. Yoo JJ, Balakrishnan K, Huang J et al (2011) Ultrathin planar graphene supercapacitors. Nano Lett 11(4):1423 1427. https://doi.org/10.1021/nl200225j
74. El-Kady MF, Strong V, Dubin S, Kaner RB (2012) Laser scribing of high-performance and flexible graphene-based electrochemical capacitors. Science 335(6074):1326–1330. https://doi.org/10.1126/science.1216744
75. Kim T, Jung G, Yoo S, Suh KS, Ruoff RS (2013) Activated graphene-based carbons as supercapacitor electrodes with macro- and mesopores. ACS Nano 7(8):6899–6905. https://doi.org/10.1021/nn402077v
76. Pope MA, Korkut S, Punckt C, Aksay IA (2013) Supercapacitor electrodes produced through evaporative consolidation of graphene oxide-water-ionic liquid gels. J Electrochem Soc 160(10):A1653–A1660. https://doi.org/10.1149/2.017310jes
77. Parvez K, Wu Z-S, Li R et al (2014) Exfoliation of graphite into graphene in aqueous solutions of inorganic salts. J Am Chem Soc 136(16):6083–6091. https://doi.org/10.1021/ja5017156
78. Purkait T, Singh G, Kumar D, Singh M, Dey RS (2018) Sci Rep 8: 640. https://doi.org/10.1038/s41598-017-18593-3
79. Li M, Pan F, Choo ESG, Lv Y, Chen Y, Xue J (2016) Designed construction of ghraphene and iron oxide freestanding electrode with enhanced flexible energy storage performance. ACS Appl Mater Interfaces 8:6972–6981. https://doi.org/10.1021/acsami.5b10853
80. Ma W, Chen S, Yang S, Chen W, Weng W, Cheng Y, Zhu M (2016) Flexible all-solid-state asymmetric supercapacitor based on transition metal oxide nanorods/reduced graphene oxide hybrid fibers with high energy density. Carbon 113:151e158. https://doi.org/10.1016/j.carbon.2016.11.051
81. Song Y, Li Z, Guo K, Shao T (2016) Hierarchically ordered mesoporous carbon/graphene composites as supercapacitor electrode materials. Nanoscale. https://doi.org/10.1039/C6NR04130B
82. Leea DG, Kim B-H (2016) MnO2 decorated on electrospun carbon nanofiber/graphene composites as supercapacitor electrode materials. Synth Met 219:115–123. https://doi.org/10.1016/j.synthmet.2016.06.007
83. Zhou S, Gao H, Zhang C, Yang J, Tang S, Xu Q, Dong S (2017) BaMF4 (M ¼ Mn, co, Ni): new electrode materials for hybrid supercapacitor with layered polar structure. J Power Sources 359:585–591. https://doi.org/10.1016/j.jpowsour.2017.05.098
84. Wang R, Han M, Zhao Q, Ren Z, Xu C, Hu N, Ning H, Song S, Lee J-M (2017) Construction of 3D CoO quantum dots/graphene hydrogels as binder-free electrodes for ultra-high energy storage applications. Electrochim Acta 686(17):31014–31019. https://doi.org/10.1016/j.electacta.2017.05.042
85. Zhou H, Liu D, Luo F, Luo B, Tia Y, Che D, Shen C (2018) Preparation of graphene nanowalls on nickel foam as supercapacitor electrodes. Micro Nano Lett 13(6):842–844b. https://doi.org/10.1049/mnl.2017.0922
86. Kumru B, Antonietti M, Schmidt BVKJ (2017) Enhanced dispersibility of graphitic carbon nitride particles in aqueous and organic media via a one-pot grafting approach, American Chemical Society. Langmuir 33:9897–9906. https://doi.org/10.1021/acs.langmuir.7b02441
87. Rok Lee Y, Kim SC, Lee H-i, Jeong HM, Raghu AV, Reddy KR, Kim BK (2011) Graphite oxides as effective fire retardants of epoxy resin. Macromol Res 19(1):66–71. https://doi.org/10.1007/s13233-011-0106-7
88. Son DR, Raghu AV, Reddy KR, Jeong HM (2016) Compatibility of thermally reduced graphene with polyesters. J Macromol Sci B: Phys 55(11):1099–1110. https://doi.org/10.1080/00222348.2016.1242529
89. Hassan M, Haque E, Reddy KR, Minett AI, Chen J, Gomes VG (2014) Edge-enriched graphene quantum dots for enhanced photo-luminescence and supercapacitance. Nanoscale 6:11988. https://doi.org/10.1039/c4nr02365j
90. Fan J, Xiao Q, Fang Y, Li L, Yuan W (2018) A rechargeable Zn/graphite dual-ion battery with an ionic liquid-based electrolyte. Ionics. https://doi.org/10.1007/s11581-018-2644-x
91. Sharma RK, Rastogi AC, Desu SB (2008) Electrochim Acta 53: 7690. https://doi.org/10.1016/j.electacta.2008.04.028
92. Simon P, Burke A (2008) Nanostructured carbons: double-layer capacitance and more. Electrochem Soc Interface 17(1):38–44 URL http://www.electrochem.org/dl/interface/spr/spr08/spr08_p38-43.pdfS
93. Wei L, Yushin G (2012) Nanostructured activated carbons from natural precursors for electrical double layer capacitors. Nano Energy 1(4):552–565. https://doi.org/10.1016/j.nanoen.2012.05.002
94. Jurewicz K, Vix-Guterl C (2004) Capacitance properties of ordered porous carbon materials prepared by a templating procedure. J Phys Chem Solids 65:287–293. https://doi.org/10.1016/j.jpcs.2003.10.024
95. Fernández J, Morishita T, Toyoda M (2008) Performance of mesoporous carbons derived from poly (vinyl alcohol) in electrochemical capacitors. J Power Sources 175:675–679. https://doi.org/10.1016/j.jpowsour.2007.09.042
96. Portet C, Taberna P, Simon P, Laberty-Robert C (2004) Modification of Al current collector surface by sol–gel deposit for carbon–carbon supercapacitor applications. Electrochim Acta 49(6):905–912. https://doi.org/10.1016/j.electacta.2003.09.043
97. Wang R, Han M, Zhao Q, Ren Z, Guo X, Xu C, Hu N, Lu L (2017) Hydrothermal synthesis of nanostructured graphene/polyaniline composites as highcapacitance electrode materials

for supercapacitors. Sci Rep 7:44562. https://doi.org/10.1038/srep44562
98. Syarif N, Tribidasari IA, Wibowo W (2013) Binder-less activated carbon electrode from gelam wood for use in supercapacitors. J Electrochem Sci Eng 3(2):37–45. https://doi.org/10.5599/jese.2012.0028
99. Andres B, Forsberg S, Vilches AP, Zhang R, Andersson H, Hummelgård M, Bäckström J, Olin H (2012) Supercapacitors with graphene coated paper electrodes. Nord Pulp Pap Res J 27(2):481
100. Roozbeh H, Niya A, Daud W, Sahu JN (2013) Preparation and characterization of activated carbon from apple waste by microwave assisted phosphoric acid. Bio Resources 8(2):2950–2966
101. Harris PF (1999) Carbon nanotubes and related structures: new materials for the twenty-first n century. Cambridge University Press, Cambridge ISBN: 0 521 55446 2
102. Journet C, Maser WK, Bernier P, Loiseau A, Lamy de la Chapelle M, Lefrant S, Deniard P, Lee R, Fischer JE (1997) Large-scale production of single-walled carbon nanotubes by the electric-arc technique. Nature 388(6644):756–758. https://doi.org/10.1038/41972
103. Ci L, Manikoth SM, Li X, Vajtai R, Ajayan PM (2007) Ultra thick freestanding aligned carbon nanotube films. Adv Mater 19(20):3300–3303. https://doi.org/10.1002/adma.200602974
104. Thess A, Lee R, Nikolaev P, Dai H, Petit P, Robert J, Xu C, Lee YH, Kim SG, Rinzler AG, Rinzler D, Colbert T, Scuseria GE, Tomanek D, Fischer JE, Smalley RE (1996) Crystalline ropes of metallic carbon nanotubes. Science 273(5274):483–487 8662534
105. Ebbesen TW, Ajayan PM (1992) Large-scale synthesis of carbon nanotubes. Nature 358(6383):220–222
106. Zheng B, Lu C, Gu G, Makarovski A, Finkelstein G, Liu J (2002) Efficient CVD growth of single-ealled carbon nanotubes on surfaces using carbon monoxide precursor. Nano Lett 2(8):895–898, and references cited therein. https://doi.org/10.1021/nl025634d
107. Shirakawa H, Louis EJ, MacDiarmid AG, Chiang CK, Heeger AJ (1977) Synthesis of electrically conducting organic polymers: halogen derivatives of polyacetylene, (CH)x. J Chem Soc, Chem Comm 1977,0,578–580. https://doi.org/10.1039/C39770000578
108. Lu W, Qu L, Dai L, Henry K (2007) Superior capacitive performance of aligned carbon nanotubes in ionic liquids. ECS Trans 6(25):257–261. https://doi.org/10.1149/1.2943245
109. Zilli D, Bonelli PR, Cukierman AL (2006) Effect of alignment on adsorption characteristics of self-oriented multi-walled carbon nanotube arrays. Nanotechnology 17(20):5136–5141. https://doi.org/10.1088/0957-4484/17/20/016
110. Talapatra S, Kar S, Pal SK, Vajtai R, Ci L, Victor P, Shaijumon MM, Kaur S, Nalamasu O, Ajayan PM (2006) Direct growth of aligned carbon nanotubes on bulk metals. Nat Nanotechnol 1(2):112–116. https://doi.org/10.1038/nnano.2006.56
111. Pushparaj VL, Shaijumon MM, Kumar A, Murugesan S, Ci L, Vajtai R et al (2007) Flexible energy storage devices based on nanocomposite paper. Proc Natl Acad Sci 104(34):13574–13577. https://doi.org/10.1073/pnas.0706508104
112. Pandolfo A, Hollenkamp A (2006) Carbon properties and their role in supercapacitors. JPowerSources 157(1):11–27. https://doi.org/10.1016/j.jpowsour.2006.02.065
113. Futaba DN, Hat K, Yamada T, Hiraoka T, Hayamizu Y, Kakudate Y, Tanaike O, Hatori H, Yumura M, Iijima S (2006) Shape-engineerable and highly densely packed single-walled carbon nanotubes and their application as super-capacitor electrodes. Nat Mater 5(12):987–994. https://doi.org/10.1038/nmat1782
114. Honda Y, Haramoto T, Takeshige M, Shiozaki H, Kitamura T, Ishikawa M (2007) Aligned MWCNT sheet electrodes prepared by transfer methodology providing high-power capacitor performance. Electrochem Solid-State Lett 10(4):A106–A110. https://doi.org/10.1149/1.2437665
115. Wang G, Zhang B, Yu Z, Qu M (2005) Manganese oxide/MWNTs composite electrodes for supercapacitors. Solid State Ionics 176(11–12):1169–1174. https://doi.org/10.1016/j.ssi.2005.02.005
116. Zhang H, Cao G, Wang Z, Yang Y, Shi Z, Gu Z (2008) Growth of manganese oxide nano flowers on vertically-aligned carbon nanotube arrays for high-rate electrochemical capacitive energy storage. Nano Lett 8(9):2664–2668. https://doi.org/10.1021/nl800925j
117. Zhang H, Cao G, Yang Y (2007) Using a cut–paste method to prepare a carbon nanotube fur electrode. Nanotechnology 18(19):195607–195610. https://doi.org/10.1088/0957-4484/18/19/195607
118. Zhang H, Cao G, Yang Y, Gu Z (2008) Comparison between electrochemical properties of aligned carbon nanotube array and entangled carbon nanotube electrodes. J Electrochem Soc 155(2):K19–K22. https://doi.org/10.1149/1.2811864
119. Lu W, Qu L, Henry K, Dai L (2009) High performance electrochemical capacitors from aligned carbon nanotube electrodes and ionic liquid electrolytes. J Power Sources 189(2):1270–1277. https://doi.org/10.1016/j.jpowsour.2009.01.009
120. Rangom Y, Tang X, Nazar LF (2015) Carbon nanotubes based supercapacitors with excellent ac line filtering and rate capability via improved interfacial impedance. ACS Nano 9(7):7248–7255. https://doi.org/10.1021/acsnano.5b02075
121. Gao L, Peng A, Wang ZY et al (2008) Growth of aligned carbon nanotube arrays on metallic substrate and its application tosupercapacitors. Solid State Commun 146(9–10):380–383. https://doi.org/10.1016/j.ssc.2008.03.034
122. Pint CL, Nicholas NW, Xu S et al (2011) Three dimensiona lsolid-state supercapacitors from aligned single-walled carbon nanotube array templates. Carbon 49(14):4890–4897. https://doi.org/10.1016/j.carbon.2011.07.011
123. Pint CL, Nicholas NW, Xu S et al (2011) Three dimensional solid-state supercapacitors from aligned single-walled carbon nanotube array templates. Carbon 49(14):4890–4897. https://doi.org/10.1016/j.carbon.2011.07.011
124. Ojha K, Kumar B, Ganguli AK (2017) Biomass derived graphene-like activated and non-activated porous carbon for advanced supercapacitors. J Chem Sci 129(3):397–404. https://doi.org/10.1007/s12039-017-1248-8
125. Dorfler S, Felhosi I, Marek T et al (2013) High power supercapelectrodes based on vertical aligned carbon nanotubes on aluminum. J Power Sources 227:218–228. https://doi.org/10.1016/j.jpowsour.2012.11.068
126. Kim B, Chung H, Kim W (2012) High-performance supercapacitors based on vertically aligned carbon nanotubes and nonaqueous electrolytes. Nanotechnology 23(15):155401. https://doi.org/10.1088/0957-4484/23/15/155401
127. Reddy KR, Lee K-P, Gopalan AI, Kim MS, Showkat AM, Nho YC (2006) Synthesis of metal (Fe or Pd)/alloy (Fe–Pd)-nanoparticles- embedded multiwall carbon nanotube/sulfonated polyaniline composites by g irradiation. J Polym Sci A Polym Chem 44:3355–3364. https://doi.org/10.1002/pola.21451
128. Hiraoka T, Izadi-Najafabadi A, Yamada T, Futaba DN, Yasuda S, Tanaike O, Hatori H, Yumura M, Iijima S, Hata K (2010) Compact and light supercapacitor electrodes from a surface-only solid by opened carbon nanotubes with 2 200 m2 g−1 surface area. Adv Funct Mater 20(3):422–428. https://doi.org/10.1002/adfm.200901927
129. Fiorentino G, Vollebregt S, Tichelaar FD, Ishihara R, Sarro PM Impact of the atomic layer deposition precursors diffusion on solid-state carbon nanotube based supercapacitors performances. Nanotechnology 26(6):064002. https://doi.org/10.1088/0957-4484/26/6/064002

130. Kaempgen M, Ma J, Gruner G, Wee G, Mhaisalkar SG (2007) Bifunctional carbon nanotube networks for supercapacitors. Appl Phys Lett 90(26):264104. https://doi.org/10.1063/1.2749187
131. Hsu Y-K, Chen Y-C, Lin Y-G, Chen L-C, Chen K-H (2012) High-cell-voltage supercapacitor of carbon nanotube/carbon cloth operating in neutral aqueous solution. J Mater Chem 22(8):3383–3387. https://doi.org/10.1039/C1JM14716A
132. Yoo Y, Kim S, Kim B, Kim W (2015) 2.5 V compact supercapacitors based on ultrathin carbon nanotube films for AC line filtering. J Mater Chem A 3(22):11801–11806. https://doi.org/10.1039/C5TA02073E
133. Du C, Yeh J, Pan N (2005) High power density supercapacitors using locally aligned carbon nanotube electrodes. Nanotechnology 16(4):350–353. https://doi.org/10.1088/0957-4484/16/4/003
134. Ghosh A, Lee YH (2012) Carbon-based electrochemical capacitors. Chem Sus Chem 5:480–499. https://doi.org/10.1002/cssc.201100645
135. Khan MU, Reddy KR, Snguanwongchai T, Haque E, Gomes VG (2016) Polymer brush synthesis on surface modified carbon nanotubes via in situ emulsion polymerization. Colloid Polym Sci 294:1599–1610. https://doi.org/10.1007/s00396-016-3922-7
136. Cakici M, Reddy KR, Alonso-Marroquin F (2016) Advanced electrochemical energy storage supercapacitors based on the flexible carbon fiber fabric-coated with uniform coral-like MnO2 structured electrodes. Chem Eng J 309(2017):151–158. https://doi.org/10.1016/j.cej.2016.10.012
137. Bello A, Fashedemi OO, Lekitima JN, Fabiane M, Dodoo-Arhin D et al (2013) High-performance symmetric electrochemical capacitor based on graphene foam and nanostructured manganese oxide. AIP Adv 3:082118. https://doi.org/10.1063/1.4819270
138. Cao X, Zheng B, Shi W, Yang J, Fan Z et al (2015) Reduced graphene oxide- wrapped MoO_3 composites prepared by using metal–organic frameworks as precursor for all-solid-state flexible supercapacitors. Adv Mater 27:4695–4701. https://doi.org/10.1002/adma.201501310
139. Gund GS, Dubal DP, Patil BH, Shinde SS, Lokhande CD (2013) Enhanced activity of chemically synthesized hybrid graphene oxide/Mn_3O_4 composite for high performance supercapacitors. Electrochim Acta 92:205–215. https://doi.org/10.1016/j.electacta.2012.12.120
140. Xie LJ, Wu JF, Chen CM, Zhang CM, Wan L et al (2013) A novel asymmetric supercapacitor with an activated carbon cathode and a reduced graphene oxide–cobalt oxide nanocomposite anode. J Power Sources 242:148–156. https://doi.org/10.1016/j.jpowsour.2013.05.081
141. Yu X, Lu B, Xu Z (2014) Super long-life supercapacitors based on the construction of nanohoneycomb-like strongly coupled CoMoO(4)-3D graphene hybrid electrodes. Adv Mater 26:1044–1051. https://doi.org/10.1002/adma.201304148
142. Peng L, Peng X, Liu B, Wu C, Xie Y et al (2013) Ultrathin two-dimensional MnO2/ graphene hybrid nanostructures for high-performance, flexible planar supercapacitors. Nano Lett 13:2151–2157. https://doi.org/10.1021/nl400600x
143. Wang CC, Chen HC, Lu SY (2014) Manganese oxide/graphene aerogel composites as an outstanding supercapacitor electrode material. Chem Eur J 20:517–523. https://doi.org/10.1002/chem.201303483
144. Kumar R, Kim HJ, Park S, Srivastava A, Oh IK (2014) Graphene-wrapped and cobalt oxide-intercalated hybrid for extremely durable super-capacitor with ultra high energy and power densities. Carbon 79:192–202. https://doi.org/10.1016/j.carbon.2014.07.059
145. Reddy KR, Hassan M, Gomes VG (2015) Hybrid nanostructures based on titanium dioxide for enhancedphotocatalysis. Appl Catal A Gen 489:1–16. https://doi.org/10.1016/j.apcata.2014.10.001
146. Du J, Zhou G, Zhang H, Cheng C, Ma J (2014) Ultrathin porous NiCo2O4 nanosheet arrays on flexible carbon fabric for high-performance supercapacitors. ACS Appl Mater Interfaces 5:7405–7409. https://doi.org/10.1021/am4017335
147. Yang W, Gao Z, Ma J, Zhang X, Wang J et al (2014) Hierarchical $NiCo_2O_4$@ NiO core–shell hetero-structured nanowire arrays on carbon cloth for a high-performance flexible all-solid-state electrochemical capacitor. J Mater Chem A 2:1448–1457. https://doi.org/10.1039/C3TA14488G
148. Huang L, Chen D, Ding Y, Feng S, Wang ZL et al (2013) Nickel-cobalt hydroxide nanosheets coated on $NiCo_2O_4$ nanowires grown on carbon fiber paper for high performance pseudocapacitors. Nano Lett 13:3135–3139. https://doi.org/10.1021/nl401086t
149. Shakir I, Shahid M, Rana UA, Al Nashef IM, Hussain R (2013) Nickel–cobalt layered double hydroxide anchored zinc oxide nanowires grown on carbon Fiber cloth for high-performance flexible Pseudocapacitive energy storage devices. Electrochim Acta 129:28–32. https://doi.org/10.1016/j.electacta.2014.02.082
150. Xiao J, Wan L, Yang S, Xiao F, Wang S (2014) Design hierarchical electrodes with highly conductive NiCo2S4 nanotube arrays grown on carbon fiber paper for high performance pseudocapacitor. Nano Lett 14:831–838. https://doi.org/10.1021/nl404199v
151. Lu X, Yu M, Zhai T, Wang G, Xie S et al (2013) High energy density asymmetric quasi-solid-state supercapacitor based on porous vanadium nitride nanowire anode. Nano Lett 13:2628–2633. https://doi.org/10.1021/nl400760a
152. Cheng S, Yang L, Liu Y, Lin W, Huang L et al (2013) Carbon fiber paper supported hybrid nanonet/nanoflower nickel oxide electrodes for high-performance pseudo capacitors. J Mater Chem A 1:7709–7716. https://doi.org/10.1039/C3TA10560A
153. Guan C, Liu J, Wang Y, Mao L, Fan Z et al (2015) Iron oxide-decorated carbon for supercapacitor anodes with ultrahigh energy density and outstanding cycling stability. ACS Nano 9:5198–5207. https://doi.org/10.1021/acsnano.5b00582
154. Hou H, Reneker DH (2004) Carbon nanotubes on carbon nanofibers: a novel structure based on electrospun polymer nanofibers. Adv Mater 16:69–73. https://doi.org/10.1002/adma.200306205
155. Ramakrishna S, Fujihara K, Teo WE, Yong T, Ma Z et al (2003) Electrospun nanofibers: solving global issues. Mater Today 9:40–50. https://doi.org/10.1016/S1369-7021(06)71389-X
156. An GH, Ahn HJ (2013) Activated porous carbon nanofibers using Sn segregation for high-performance electrochemical capacitors. Carbon 65:87–96. https://doi.org/10.1016/j.carbon.2013.08.002
157. Zhang F, Yuan C, Zhu J, Wang J, Zhang X et al (2013) Flexible films derived from electrospun carbon nanofibers incorporated with Co3O4 hollow nanoparticles as self-supported electrodes for electrochemical capacitors. Adv Funct Mater 23:3909–3915. https://doi.org/10.1002/adfm.201203844
158. Kim BH, Yang KS, Yang DJ (2013) Electrochemical behavior of activated carbon nanofiber-vanadium pentoxide composites for double-layer capacitors. Electrochim Acta 109:859–865. https://doi.org/10.1016/j.electacta.2013.07.180
159. Kim CH, Kim BH (2015) Zinc oxide/activated carbon nanofiber composites for highperformance supercapacitor electrodes. J Power Sources 274:512–520. https://doi.org/10.1016/j.jpowsour.2014.10.126
160. Kim C, Yang K (2003) Electrochemical properties of carbon nanofiber web as an electrode for supercapacitor prepared by electrospinning. Appl Phys Lett 83:1216–1218. https://doi.org/10.1063/1.1599963
161. Wang W, Guo S, Lee I, Ahmed K, Zhong J et al (2014) Hydrous ruthenium oxide nanoparticles anchored to graphene and carbon nanotube hybrid foam for supercapacitors. Sci Rep 4:4452. https://doi.org/10.1038/srep04452

162. He Y, Chen W, Zhou J, Li X, Tang P et al (2013) Constructed uninterrupted charge transfer pathways in three-dimensional micro/nano interconnected carbon-based electrodes for high energy-density ultra light flexible supercapacitors. ACS Appl Mater Interfaces 6:210–218. https://doi.org/10.1021/am403760h
163. Sawangphruk M, Srimuk P, Chiochan P, Krittayavathananon A, Luanwuthi S et al (2013) High-performance supercapacitor of manganese oxide/reduced graphene oxide nanocomposite coated on flexible carbon fiber paper. Carbon 60:109–116. https://doi.org/10.1016/j.carbon.2013.03.062
164. Zhang LL, Xiong Z, Zhao XA (2013) Composite electrode consisting of nickel hydroxide, carbon nanotubes, and reduced graphene oxide with an ultrahigh electrocapacitance. J Power Sources 222:326–332. https://doi.org/10.1016/j.jpowsour.2012.09.016
165. Zhu C, Yang P, Chao D, Wang X, Zhang X et al (2015) All metal nitrides solid-state asymmetric supercapacitors. Adv Mater 27:4566–4571. https://doi.org/10.1002/adma.201501838
166. Wang JG, Yang Y, Huang ZH, Kang F (2013) A high-performance asymmetric supercapacitor based on carbon and carbon–MnO 2 nanofiber electrodes. Carbon 6:190–199. https://doi.org/10.1016/j.carbon.2013.04.084